HHS Public Access

Author manuscript

Dev Cell. Author manuscript; available in PMC 2022 August 09.

Published in final edited form as:

Dev Cell. 2021 August 09; 56(15): 2160–2175.e5. doi:10.1016/j.devcel.2021.06.020.

Proteolytic activation of Growth-Blocking Peptides triggers calcium responses through the GPCR Mthl10 during epithelial wound detection

James T. O'Connor[1,2], **Aaron C. Stevens**[3], **Erica K. Shannon**[1,2], **Fabiha Bushra Akbar**[1,4], **Kimberly S. LaFever**[1], **Neil P. Narayanan**[1,5], **Casey D. Gailey**[1], **M. Shane Hutson**[3,6,7,*], **Andrea Page-McCaw**[1,2,8,9,*]

[1]Department of Cell and Developmental Biology, Vanderbilt University, Nashville, Tennessee

[2]Program in Developmental Biology, Vanderbilt University, Nashville, Tennessee

[3]Department of Physics and Astronomy, Vanderbilt University, Nashville, Tennessee

[4]University of Chicago, Chicago, Illinois

[5]University School of Nashville, Nashville, Tennessee

[6]Department of Biological Sciences, Vanderbilt University, Nashville, Tennessee

[7]Institute for Integrative Biosystems Research and Education, Vanderbilt University, Nashville, Tennessee

[8]Vanderbilt-Ingram Cancer Center, Vanderbilt University, Nashville, Tennessee

[9]Lead Contact

Summary

The presence of a wound triggers surrounding cells to initiate repair mechanisms, but it is not clear how cells initially detect wounds. In epithelial cells, the earliest known wound response, occurring within seconds, is a dramatic increase in cytosolic calcium. Here we show that wounds in the *Drosophila* notum trigger cytoplasmic calcium increase by activating extracellular cytokines, Growth-blocking peptides (Gbps), which initiate signaling in surrounding epithelial cells through the G-protein coupled receptor, Methuselah-like 10 (Mthl10). Latent Gbps are present in unwounded tissue and are activated by proteolytic cleavage. Using wing discs, we show that multiple protease families can activate Gbps, suggesting they act as a generalized protease-

[*]Authors for correspondence: andrea.page-mccaw@vanderbilt.edu, shane.hutson@vanderbilt.edu.

Author Contributions

J.O.C., E.K.S., A.C.S., M.S.H., and A.P.M designed this study and developed the methodology for experiments. K.S.L. and N.N. created the $Gbp1^{\Delta}$ and $Gbp2^{3\Delta FS}$ mutant fly lines. J.O.C., E.K.S., and C.D.G. performed pupal wounding experiments and analyzed that data. J.O.C. and F.B.A. performed larval wing disc experiments and analyzed that data. A.C.S. and M.S.H. designed and created the computational model. J.O.C. and A.C.S. created the figures. J.O.C., A.C.S., M.S.H., and A.P.M. wrote and edited the manuscript.

Declaration of Interests

The authors declare no competing interests.

detector system. We present experimental and computational evidence that proteases released during wound-induced cell damage and lysis serve as the instructive signal: these proteases liberate Gbp ligands, which bind to Mthl10 receptors on surrounding epithelial cells, and activate downstream release of calcium.

eTOC Blurb

O'Connor, et al. investigate how cells in an epithelium detect the presence of nearby wounds. The mechanism is initiated by proteases released from lysing cells, which activate latent proligand cytokines. These rapidly signal to nearby cells to increase cytosolic calcium known to aid in the wound response.

Graphical Abstract

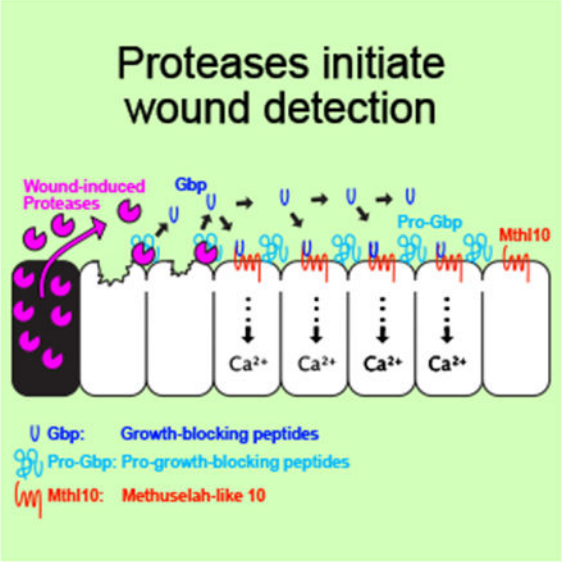

Introduction

When a tissue is wounded, the cells surrounding the wound rapidly respond to repair the damage. Despite the non-specific nature of cellular damage, there is remarkable specificity to the earliest cellular response: cells around the wound increase cytosolic calcium, and this damage response is conserved across the animal kingdom (Antunes et al., 2013; Enyedi et al., 2016; Hunter et al., 2015, 2018; Klepeis et al., 2001; Razzell et al., 2013; Shabir and Southgate, 2008; Shannon et al., 2017; Stanisstreet, 1982; Tu et al., 2019; Xu and Chisholm, 2011; Yoo et al., 2012). The calcium response is not limited to cells at the wound margin, but extends even to distal cells (Antunes et al., 2013; Enyedi et al., 2016; Razzell et al., 2013; Yoo et al., 2012). Multiple molecular mechanisms have been identified that regulate wound-induced gene expression or cell behavior downstream of calcium (Antunes et al., 2013; Benink and Bement, 2005; Enyedi et al., 2016; Gao et al., 2013; Hander et al., 2019; McNeil and Steinhardt, 2003; Razzell et al., 2013; Wu et al., 2009; Yoo et al., 2012), but the

upstream signals remain unclear. How exactly do cells detect wounds? Here we investigate the molecular mechanisms by which a wound initiates cytosolic calcium signals.

The immediate increase in cellular calcium in turn initiates repair or defense responses. Calcium has been well-established as a versatile and universal intracellular signal that plays a role in the modulation of numerous intracellular processes. Several calcium-regulated processes are required for proper wound repair, including actomyosin dynamics (Antunes et al., 2013; Benink and Bement, 2005; Kong et al., 2019; Levy and Ryan, 1965; Martin and Lewis, 1992; Wales et al., 2016), JNK pathway activation (Gao et al., 2013) and plasma membrane repair (reviewed in Cooper and McNeil, 2015). Unsurprisingly, an increase in cytosolic calcium is necessary for wound repair (Benink and Bement, 2005; McNeil and Steinhardt, 2003; Shabir and Southgate, 2008; Xu and Chisholm, 2011; Yoo et al., 2012).

Nonetheless, there is less clarity on the mechanisms that trigger increased cytosolic calcium in cells near to and distant from the wound. In some cases, wound-induced cytoplasmic calcium enters from the extracellular environment, either directly through plasma membrane damage (Benink and Bement, 2005; Gao et al., 2013; McNeil and Steinhardt, 2003; Shabir and Southgate, 2008; Shannon et al., 2017; Stanisstreet, 1982) or through calcium ion channels like TrpM (Antunes et al., 2013; Razzell et al., 2013; Xu and Chisholm, 2011). In others, calcium is released from the endoplasmic reticulum (ER) through the IP_3 Receptor (Klepeis et al., 2001; Narciso et al., 2015; Restrepo and Basler, 2016; Shabir and Southgate, 2008; Tu et al., 2019; Xu and Chisholm, 2011), and initiated by an unknown G-Protein Coupled Receptor (GPCR) or Receptor Tyrosine Kinase (RTK). Further, calcium responses can be initiated by mechanical stimuli alone (D'hondt et al., 2013; Gomes et al., 2003; Narciso et al., 2017; Restrepo and Basler, 2016). Elucidating the mechanisms by which calcium signaling is triggered *in vivo* is critical to understanding how wound information is transmitted through a tissue in order to change cellular behavior and properly repair the wound.

By live imaging laser wounds in *Drosophila* pupae, we previously showed that damaged cells around wounds become flooded within milliseconds by extracellular calcium entering through microtears in the plasma membrane (Shannon et al., 2017). Although this calcium influx expands one or two cell diameters through gap junctions, it does not extend to more distal cells. Strikingly, after a delay of 45-75 seconds, a second independent calcium response expands outward to reach a larger number of distal cells. Here we identify the relevant signal transduction pathway and receptor, the GPCR Mthl10. Downstream, signals are relayed through Gαq and PLCβ to release calcium from the ER. Upstream, Mthl10 is activated around wounds by the cytokine ligands Growth-blocking peptides (Gbps). Further, we provide experimental and computational evidence that the initiating event for the distal calcium response *in vivo* is a wound-induced release of proteases that activate the latent Gbp cytokines, cleaving them from inactive/pro-forms into active signaling molecules.

Results

To investigate the calcium responses after wounding, we analyzed *Drosophila* pupae (Fig. 1A), which are amenable to live imaging *in vivo* because they are stationary throughout

development. By partially removing the pupal case, we were able to access and wound the epithelial monolayer of the dorsal thorax, termed the notum (Fig 1A, white box). After wounding and imaging, nearly all wild-type pupae recovered to eclose as adults.

The calcium responses observed after wounding are temporally and spatially complex and somewhat variable (Shannon et al., 2017), making it more difficult to identify underlying mechanisms by comparing wild-type and mutant animals. To circumvent this problem, we exploited the radial symmetry of the calcium response by manipulating gene expression on only one side of the wound, allowing us to assess symmetry in control versus experimental regions. We used the *Gal4/UAS* system to manipulate gene expression in the central region of the notum with *pnr-Gal4* (Fig. 1A'), and then wounded on the margin between the control and knock-down region, so that half the wound served as an internal control (Fig. 1B, C). We monitored the symmetry of the calcium responses with a ubiquitously expressed calcium reporter, *ActinP-GCaMP6m*, comparing the experimental (*pnr*) domain with the adjacent internal control. When no other genes are manipulated, the calcium signals remain radially symmetric about the wound (Fig. 1D, Movie 1).

The distal calcium response signals to release calcium via IP_3.

We first used this internally controlled system to knock down gap junctions, which we have previously shown to be required for the first calcium expansion (Shannon et al., 2017). As expected, the first expansion did not occur in the gap junction knockdown region but did in the control region (Fig. S1A). Importantly, the second distal calcium response still occurred in the gap junction knockdown region, although it appeared "speckled" because each cell transduced the signal independently of its neighbors (Fig. S1A), as has been reported previously (Balaji et al., 2017; Restrepo and Basler, 2016; Shannon et al., 2017). This result indicated that the initiation of the distal calcium response requires neither gap junctions nor the first (gap junction-dependent) expansion.

To determine whether the calcium of the distal response was coming from internal stores within the cell, we knocked down IP_3 Receptor (IP_3R), which controls calcium release from the endoplasmic reticulum. Knocking down IP_3R on one side of the wound using our internally-controlled system demonstrated that it is absolutely required for the distal calcium response (Fig. 1E). Importantly, the effect was limited to the experimental domain, while the control domain calcium response remained intact. We confirmed this result with two independent RNAi lines and an IP_3 sponge (Fig. S1B) and concluded that calcium is released from intracellular stores in an IP_3-dependent manner.

The IP_3 signal transduction pathway has been well studied. IP_3 is generated via hydrolysis of phosphatidylinositol 4,5-bisphosphate (PIP_2) into IP_3 and diacylglycerol (DAG), a reaction catalyzed by the enzyme phospholipase C beta (PLCβ). To test the role of PLCβ, we knocked it down on one side of the wound and found that PLCβ is required for the distal calcium response (Fig. 1F). This result was obtained with two independent RNAi lines. As the next step upstream, PLCβ is most commonly activated through the G_q-signaling pathway; activation of a G-protein coupled receptor causes the α-subunit of the G_q-heterotrimer (known as Gαq) to dissociate from its β and γ subunits to activate PLCβ. Indeed, previous literature studying IP_3-mediated calcium responses following injury have

also implicated Gαq (Weinger et al., 2005; Xu and Chisholm, 2011). To test the role of G_q-signaling, we knocked down Gαq on one side of the wound and found that it was also required for the distal calcium response (Fig. 1G, Movie 2). These results demonstrate that the distal calcium response is transduced via the canonical G_q-signaling pathway.

Importantly, although all of the above experiments used laser wounding, we find that puncture wounds also had two distinct calcium waves: the first occurred immediately and required gap junctions; the second was delayed by tens of seconds and similarly required the G_q pathway (Movie 3). Thus, the mechanisms underlying the two calcium responses appear to be general wound responses, not specific to laser ablation.

Interestingly, a modification of our internally controlled system suggests that wound-induced signals can diffuse in the extracellular space. Rather than wounding on the *pnr* domain border, we wounded in the middle of a *pnr* domain where Gαq was knocked down. As expected, no distal calcium response occurred within the knockdown domain, but the calcium response did jump the gap of knockdown cells to suddenly appear in the even more distal control domain (Fig. 1H, Movie 4).

To quantify how gene knockdown alters the distal calcium response, we calculated the difference in maximum calcium-signal radius in the control and experimental regions (illustrated in 1E'). Each G_q-pathway knockdown significantly inhibited the calcium response (Fig. 1I). Taken together, the distal calcium response occurs through a G_q-signaling pathway likely activated by a diffusible signal.

The distal calcium response requires the GPCR Mthl10.

The requirement of G_q suggested that the distal calcium response is initiated by a GPCR; however, given previous reports that the TrpM ion channel could alter the intensity of wound-induced calcium responses in the pupal notum (Antunes et al., 2013; Razzell et al., 2013; Xu and Chisholm, 2011), we first knocked down TrpM with either of two previously-used functional RNAi lines. Neither had a discernible effect on the timing or range of the calcium response: the experimental domain remained symmetrical to its internal control (Fig. 2A, D). Next, we knocked down candidate GPCRs, prioritizing receptors with known epithelial expression and G_q activity (Hanlon and Andrew, 2015). Previous cell-culture studies have implicated ATP as a ligand activating calcium after wounding (Weinger et al., 2005), and a recent study in mice implicated ADP in intercellular calcium waves following viral infection (Chang-Graham et al., 2020). We thus knocked down *AdoR*, the only *Drosophila* adenosine receptor, but it had no effect on the calcium response (Fig. 2B, D). We then knocked down the GPCRs *Tre1* or *TkR86C*, both implicated in wound responses (Thuma et al., 2018; Yang et al., 2014), but they also had no effect on the calcium response (Fig. 2D). Strikingly, we were able to completely eliminate the distal calcium responses by knocking down the cytokine-activated GPCR *Methuselah-like 10 (Mthl10)* (Sung et al., 2017) (Fig. 2C, D, Movie 5). We confirmed this result with two independent RNAi lines. To test whether *Mthl10* is important for wound recovery, we measured pupal survival after large wounds and found that *Mthl10* knockdown throughout the notum decreased pupal survival by ~30% (Fig. 2E).

Mthl10 is activated by Gbp1 and Gbp2.

Mthl10 is known to be activated by a class of cytokines known as Growth-blocking peptides (Gbps), of which there are five in *Drosophila* (Sung et al., 2017; Tsuzuki et al., 2012). Gbps are synthesized in the *Drosophila* fat body in a latent pro-peptide form, requiring proteolytic cleavage for activation (Endo et al., 1998; Hayakawa, 1991; Matsumoto et al., 2003; Shears and Hayakawa, 2019; Tsuzuki et al., 2012). Because Gbps are secreted (and thus not cell-autonomous), the internally controlled knockdown approach expressing an RNAi exclusively in epithelial cells would not be effective at testing their role; we instead needed to test homozygous Gbp knockout pupae. We used CRISPR to generate individual null mutants of *Gbp1* or *Gbp2* (hereafter referred to as $Gbp1^{\Delta}$ and $Gbp2^{3\Delta FS}$, respectively; Fig. 3A), and obtained the previously generated and homozygous viable strain *Df(2R)Gbp-ex67*, which has a small chromosomal deletion removing the neighboring genes *Gbp1* and *Gbp2* (Koyama and Mirth, 2016) (hereafter referred to as Δ*Gbp1,2;* Fig. 3A). Upon wounding these animals, we found the individual null mutants of *Gbp1* or *Gbp2* did not appear to have an altered calcium response compared to control (Fig. 3B–D). However, the Δ*Gbp1,2* pupae lacked a normal distal calcium response in 13 out of 14 pupae (Fig. 3E).

Because this method does not have an internal control, we analyzed the spatiotemporal dynamics of the distal calcium responses using the following metrics: (1) its relative spatial extent via $(R_{Max} - R_{1st})/R_{1st}$, where R_{Max} is the maximum calcium-signal radius and R_{1st} is the radius of the first expansion (illustrated in Fig. 3B'), which provides normalization for wound size (Fig. 3G); (2) its duration via the time over which the calcium-signal radius remained greater than R_{1st}(Fig. 3H); and (3) its start time (Fig. 3I). The spatial quantification showed that Δ*Gbp1,2* significantly reduces the radius of the distal calcium response. The vast majority of Δ*Gbp1,2* samples actually had values at or near zero because there was no distal expansion. On the other hand, the individual null mutants had robust distal expansions that were not significantly different from controls (Fig. 3G). We obtained similar results for quantification of the distal calcium response duration: Δ*Gbp1,2* signal duration was significantly reduced compared to control (Fig. 3H), whereas that of the individual nulls was either unchanged ($Gbp1^{\Delta}$) or even increased (*Gbp2*$^{3\Delta FS}$). In those samples for which there was a distal calcium response, none of the nulls showed a significant difference in the response start time (Fig. 3I).

Taken together, this data shows that the absence of both *Gbp1* and *Gbp2* significantly decreases the response radius and duration, while that of *Gbp1* or *Gbp2* alone does not. Each extracellular ligand, Gbp1 or Gbp2, is independently sufficient to relay wound information to surrounding cells.

If Gbps are wound-induced signals that direct cells to increase calcium, then ectopic Gbp would be expected to activate a calcium response, even without a wound. Unfortunately, the pupal notum is protected by an impermeable cuticle that makes it impossible to add Gbp directly to the tissue, and it cannot be removed without wounding. We thus turned to larval wing discs, sacs of epithelial tissue that have no cuticle. We applied synthetic active-form Gbp peptides directly to wing discs *ex vivo* at varying concentrations. Excitingly, we found that both Gbp1 and Gbp2 elicited a strong calcium response in wing discs when added *ex vivo* at 5 nM or 50 nM, respectively (Fig. 4A, B). To test whether these responses were

Mthl10-dependent, we mounted one control and one *Mthl10* knockdown disc side-by-side in a media bubble and added Gbp peptide to both discs simultaneously. As expected, the calcium responses were absent from the *Mthl10* knockdown discs (Fig. 4C, D, Movie 6). Finally, we asked whether the three other Gbps could elicit calcium in wing discs and found that Gbp4 and Gbp5 could elicit calcium consistently at 50 nM (and Gbp4 occasionally even at 5 nM), while Gbp3 was not effective, even at 50 μM, the maximum concentration tested (Fig. S2). Despite the activity of these other Gbps *ex vivo*, the loss of the distal calcium response in the Δ*Gbp1,2* pupae indicates Gbp1 and Gbp2 are responsible for the calcium increase in the pupal notum.

Gbps and Mthl10 are required for calcium waves in wing discs.

Previous studies have shown that wing discs cultured *ex vivo* displayed potent calcium responses upon exposure to fly extract (Balaji et al., 2017; Narciso et al., 2017; Restrepo and Basler, 2016). Because fly extract is created by lysing and homogenizing whole flies, we hypothesized that it contained wound-induced signals that activate wound-detection pathways in wing discs to initiate calcium responses. Indeed, we observed the calcium response was *mthl10*-dependent by adding fly extract to control and *mthl10* knockdown wing discs simultaneously (Fig. 4F, H, Movie 7). Since extract of adult flies is predicted to contain both Gbp4 and Gbp5, which may be confounding variables, we also tested extract made from larvae, a stage that expresses only Gpb1-3 (Tsuzuki et al., 2012); like adult extract, wild-type larval extract activated calcium responses in wing discs in an *mthl10*-dependent manner (Fig. 4G, H, Movie 7). This shows that, in addition to the distal calcium response following wounding, Mthl10 mediates the lysate-induced calcium response in wing discs.

To determine whether the calcium-activating signal in the extract is Gbp, we added extract made from either wild-type or homozygous Δ*Gbp1,2* larvae to either control or homozygous Δ*Gpb1,2* wing discs (Fig. 5A, B). We found that no calcium response occurs when Gbps are absent from both disc and extract (Fig. 5B, C, Movie 8), demonstrating that the calcium response to larval extract does indeed require Gbp1 and/or Gbp2. Surprisingly, as long as Gbp was present in either the extract or the disc, the extract was able to elicit a calcium response. (Fig. 5A–C, Movie 8). The former result is expected: extract made from wild-type larvae contains Gbp, which elicits calcium when applied to wing discs. The latter result is less intuitive and suggests that the wing discs themselves maintain a local supply of Gbp that can be activated by larval extract. If the discs already have Gbp, then what does the extract provide to activate calcium? This result suggested that proteases in the extract are necessary to cleave latent pro-Gbp from the disc to elicit the calcium response.

Gbps are activated by multiple proteases.

Bioinformatics analysis predicted that both pro-Gbp1 and pro-Gbp2 could release their active C-terminal peptides after cleavage by several unrelated proteases (Gasteiger et al., 2003). To confirm the activity of proteases in the lysate, we tried to inhibit them using broad-spectrum protease inhibitors, singly and in combination. Unfortunately, the inhibitors or the vehicle (DMSO) alone at high enough concentrations could themselves induce calcium responses in wing discs, stymieing our ability to use inhibitors in this experiment.

As an alternative approach, we noted that the serine protease trypsin and the cysteine protease clostripain are both predicted to cleave Gbp1 (Gasteiger et al., 2003). To test their ability to activate calcium in wing discs, we added trypsin or clostripain to wing discs and found that each was sufficient to elicit a calcium response in control but not Δ*Gbp1,2* wing discs (Fig. 5D–F). Given that cell lysis is known to release multiple active proteases, our data suggest a model in which wound detection in the *Drosophila* notum depends on latent pro-Gbps in the extracellular space, acting as protease detectors, reporting the presence of wound-induced cell lysis via Mthl10 signaling.

Enzymatic generation of a diffusible signal explains wound-size dependence

This protease/Gbp/Mthl10 model is substantially more complex than the delayed-diffusion model of an unknown signal we presented previously (Shannon et al., 2017). That initial model was based on instantaneous release and diffusive spread of a single, unknown wound-induced signal. Although it lacked mechanistic detail, the prior model fit the data well and provided a useful parameterization of response dynamics: a total amount of signal released compared to its detection threshold (M/C_{th}), a back-propagated time delay $t_{0,min}$ at which calcium signals first become apparent, and an effective diffusion constant α_{eff} describing the rate at which signal spreads distally. A close look at these fitted parameters shows that the time delay and effective diffusion constant have definite trends with wound size (Fig. 6F,F'; $n = 26$ wounds with diameters > 15 μm).

The delayed-diffusion model can describe these trends, but the description does not provide explanatory power. We find that α_{eff} increases linearly with wound diameter w:

$$\alpha_{\mathrm{eff}} = (0.77 \pm 0.26\ \mu\mathrm{m/s})w - (8 \pm 11\ \mu\mathrm{m}^2/s),$$

whereas the trend for $t_{0,min}$ is better described by a linear dependence on $1/w$:

$$t_{0,\,\mathrm{min}} = (1500 \pm 700\ \mu\mathrm{m\ s})w^{-1} + (12 \pm 19\ \mathrm{s})\,.$$

The coefficients of the w or $1/w$ term are non-zero (with p-values of 0.006 and 0.04, respectively). Although one can postulate explanatory hypotheses, the delayed-diffusion model itself provides no reason for the wound-size dependence of the response dynamics. We thus wanted to explore whether the observed trends would fall out naturally from a more detailed model based on the protease/Gbp mechanism.

To do so, we constructed a computational reaction-diffusion model as outlined in Fig. 6A, A'. In brief, wound-induced cell lysis releases proteases that enzymatically cleave extracellular pro-Gbps into their active forms, which then reversibly bind Mthl10 receptors. This abstraction treats all classes of proteases as a single pool of temporally and spatially varying protease activity. It also pools all Gbp family members, but does keep track of pro- and active forms. Because Mthl10 is membrane bound, and pro-Gbp2 physically interacts with collagen IV (Guruharsha et al., 2011), both species are treated as stationary in the model, but released proteases and active Gbps are allowed to diffuse. The model is solved over time and a 2D radially symmetric space for six species – protease, free active Gbp,

and receptor-bound Gbp (Fig. 6B), as well as pro-Gbp, protease::pro-Gbp complex and free receptor. Signaling downstream of the receptor is approximated as a threshold event that releases calcium from intracellular stores when a given fraction of receptors are bound by ligand (Fig. 6C, dashed line). For complete mathematical details, see Supporting Text.

As constructed, this model has nine free parameters including protease release characteristics, initial component concentrations, diffusion constants, and reaction rates (see Reaction-Diffusion Model supplemental text and Fig. S5). Given that experimental response dynamics are adequately fit by a simpler model using just three parameters, one should not expect fits of the more detailed model to place strong constraints on all parameters. Instead, the detailed model falls into the category of "soft" or "sloppy" behavior common in systems biology (Gutenkunst et al., 2007): parameters are weakly constrained, often varying over orders of magnitude, but predictions of model output are nonetheless robust and useful. In an attempt to provide stronger parameter constraints, we did try simultaneous fitting of multiple experimental data sets using a set of nine shared parameter values. Such fits did not describe the data well (Fig. S3A). As a second attempt, recognizing that wound size varied among experiments, we also tried simultaneous, multiple-data-set fits using seven shared biochemical parameter values and two experiment-specific wound parameters; however, this additional flexibility was still insufficient (Fig. S3B). We thus proceeded with fits of the full nine-parameter model to individual data sets and used the resulting parameter sets as the basis for comparing further model predictions with experimental data.

We selected four typical distal calcium responses and fit each calcium signal radius versus time to the reaction-diffusion model using a constrained least-squares approach (see Supporting Text). For each experimental response, we conducted 32 fits with different randomly selected sets of initial parameter guesses. We used the single best fit to estimate the variance and kept all fits for which the chi-squared statistic indicated an equivalently good fit at the 95% confidence level (3-7 fits for each experiment). A single experimental response and model fit are shown in Fig. 6D, and a full grid of all good fits is shown in Fig. S4A. As expected for a "soft" model, the superset of parameter estimates from all good fits yields distributions for individual parameters that vary by orders of magnitude (Fig. S4B).

Despite these variations among best-fit parameters, the model makes robust predictions for its output's dependence on wound size. For each set of best fit parameters (a set being a group of nine parameters that yield a good fit), we solved the model with all parameters fixed, save two that scale with wound size: the $1/e^2$ radius of the protease source, which scales linearly with wound radius; and the total amount of protease activity released, which scales as wound radius squared. With these two parameters scaled in this manner, the peak density of the protease source (activity released per unit area) is held constant. As the example in Fig. 6E shows, increasing wound size in the model yields smaller time delays and more rapid diffusion-like signal spread. To better compare to experimental trends, we parameterized the detailed model output in the same way as experimental data, i.e., by fitting its calcium signal radius versus time to the three-parameter delayed-diffusion model. The resulting wound-size dependencies fall out as two natural predictions of the detailed model. First, the parameterization shows that the effective diffusion constant in the detailed model output increases with wound size around every one of the widely varying best-fit parameter

sets (each colored line in Fig. 6F). Although individual curves flatten out as α approaches zero, the trends are mostly linear and the slopes are comparable or greater than the trend observed across all experiments. Second, the parameterization shows that the signaling time delay in the detailed model varies in a roughly hyperbolic manner with wound size. These predicted trends are also similar to experiments (Fig. 6F').

Within the detailed model, the wound-size-dependence for the time delay and spread rate of the distal response can be traced to a generalized mechanism with two key structural features. First, the signal (i.e., active Gbp) builds up gradually over time. Second, the signal diffuses rapidly enough during this build up to spread well beyond the spatial extent of its source. The first feature by itself provides both a time delay associated with reaching threshold and a diffusion-like spread associated with the threshold boundary moving further from the wound as signal builds; however, it does not yield a wound-size dependence. Even though smaller wounds produce smaller amounts of protease activity and thus smaller integrated signals, they do so over smaller areas to yield the same signal density as larger wounds. The second key structural feature, relatively rapid diffusional spread, ensures that signals from small or large wounds are spread over comparable areas, decreasing the signal density for smaller wounds, increasing it for larger wounds. This signal density difference yields the observed wound-size dependence for α and $t_{0,\min}$.

Using the computational model, we are able to recapitulate key features of the calcium response. For example, we modeled the same parameters in a control vs a 70% reduction in Mthl10 levels (Fig. 7A) and found this matches the observed response in our internally-controlled system where Mthl10 is knocked down on one side of the wound while an internal control is maintained (Fig. 7B). We also modelled variations of extracellular pro-Gbp levels and found that, for the best-fit parameter sets, decreasing pro-Gbp levels are predicted to decrease the spatial extent and duration of the calcium response (four model output examples shown in Fig. 7C). In experiments, we observed similarly modified responses in the double null Δ*Gbp1,2*, but not in the individual null mutants of *Gbp1* or *Gbp2* (Fig. 3). Since the Gbp reduction in individual nulls was perhaps insufficient to measurably alter the calcium response, we revisited this experiment using trans-heterozygotes of the Δ*Gbp1,2* deletion and one of the individual null mutant alleles ($Gbp1^{\Delta}$ or $Gbp2^{3\Delta FS}$). The resultant pupae expressed only one allele of *Gbp1* and were null for Gbp2 ($\Delta Gbp1,2/Gbp2^{3\Delta FS}$) or expressed one allele of *Gbp2* and were null for *Gbp1* ($\Delta Gbp1,2/Gbp1^{\Delta}$). We wounded each of these pupae and compared their distal calcium responses to controls and found that the spatial extent was significantly decreased in both conditions compared to controls (Fig. 7D). Furthermore, the response duration was decreased significantly in the pupae null for *Gbp1* and heterozygous for *Gbp2* (Fig. 7E). Interestingly, the start times (Fig. 7F) were not significantly different in either condition, which matches the very weak dependence of start time on Gbp levels in the model (Fig. 7C). These results experimentally validate the model prediction that sufficient reduction in pro-Gbp prior to wounding can decrease the spatial extent and duration of the calcium response.

Computational model identifies key role for cell lysis over time

In the detailed model construction used here (Fig. 6A), the rate of signal spread is controlled largely by the rate of signal accumulation plus the diffusion constant of active Gbp. Diffusive spread of the protease itself is minimal (Fig. 6B). The rate of signal accumulation itself is controlled by the rate constant for the release of protease activity via cell lysis, k_S, and the enzymatic rate constant for proteolytic cleavage of pro-Gbp, k_C. Among the set of best fits, these two model parameters can compensate for one another, as shown by their inverse correlation (Fig. 7G). One can be fast so long as the other serves as the sufficiently slow rate-limiting step in generating active Gbp. In most best-fit parameter sets, the rate-limiting step had a corresponding time constant ($1/k$) of 50-500 s. Interestingly, only a few of the best fits had a quick release of protease activity after wounding ($1/k_S$ < 1 s) and modifying the model to force an instantaneous release of this activity failed to fit the experimental data. In other words, the model predicts that extracellular protease release occurs progressively over time after wounding, rather than all at once. Given that laser-induced wounds are made very rapidly – cavitation bubble generation and collapse occur within microseconds – the best-fits' requirement for much slower protease release was an unexpected prediction. We hypothesized that the key step may not be an instantaneous release of proteases from all damaged cells, but rather slow and progressive cell lysis. This led us to reexamine live imaging of nuclear-mCherry-labeled cells around wounds. Although a small number of cells were destroyed immediately by the ablation process, a much larger group of surrounding cells were observed to lyse progressively over ~90 seconds, validating the model's prediction that the wound-induced cell destruction is not instantaneous (Fig. 7H).

Quantitative modeling based on the protease/Gbp mechanism thus provides explanations for the distal calcium response's wound-size dependencies, makes verified predictions regarding required extracellular pro-Gbp concentrations, and makes an unanticipated prediction about slow protease release that matches a reexamination of experimental data. Further model predictions are provided by the sensitivity analysis shown in Fig. S5. Several parameters have a strong impact on the timing and reach of the distal calcium response, including all those related to the release of protease activity, plus the rate constant for pro-Gbp cleavage, and the initial amount of pro-Gbp present in the extracellular space. It is especially interesting that the amounts of pro-Gbps have a strong impact on the calcium response, as these are known to vary with environmental conditions (Koyama and Mirth, 2016). The inclusion of an extracellular enzymatic step in the wound-detection pathway provides both signal amplification and multiple options for regulation. Quantitative modeling provides a set of potentially experimentally testable predictions for how this regulation could function *in vivo.*

Discussion

This study traces the induction of the repair process back to the wound itself. We find that for epithelial wounds in the *Drosophila* notum, the cell-surface receptor Mthl10 responds to Gbp ligands in the extracellular environment, triggering a cell-autonomous increase in cytoplasmic calcium. It was already known that Gbps are synthesized in an inactive

pro-form, requiring proteolytic cleavage for activation, and that they are secreted by the fat body. We find that although Gbps are present in unwounded tissues, they activate Mthl10 only in the presence of a wound. Interestingly, Gbps have cleavage consensus sequences for multiple protease families. Further, the addition of cell lysate or the addition of the unrelated proteases trypsin or clostripain to unwounded tissue is sufficient to generate a calcium signal in wing discs through Mthl10/Gbp signaling. These results lead us to a model in which the lysis of cells inherent in wounding releases non-specific cellular proteases into the extracellular environment. These proteases cleave and activate extracellular Gbps, which in turn activate the Mthl10 GPCR on cells around the wound, initiating wound-induced calcium signaling. Such cell lysis and protease release should be a general feature of cell destruction, whether caused by trauma, pathogen-induced lysis, or a lytic form of cell death such as pyroptosis or necroptosis (immunologically silent apoptosis may well be an exception (Frank and Vince, 2019)). A variety of epithelial damage mechanisms may thus converge through the Gbps to signal via the GPCR Mthl10 and alert surrounding cells to the presence of a nearby wound. This molecular mechanism is supported by a computational model which accurately describes the pattern and timing of wound-induced calcium, predicted its dependence on wound size and initial levels of Gbps, and directed us to observe that cell lysis is not immediate but rather takes place over 10s of seconds. Thus, we offer a model for how surrounding cells detect the damage of cell lysis, utilizing a Gbp-based protease detector system.

Two superimposed mechanisms increase cytoplasmic calcium levels around wounds.

Laser-wounds generate complex yet reproducible patterns of increased cytoplasmic calcium, and the complexity of this pattern has undoubtedly made it difficult to unravel its underlying mechanisms. Within the first ~90 seconds after wounding, two mechanisms drive the increase of calcium, and the complexity is generated by the temporal and spatial superimposition of these two mechanisms. Previously, we reported that a different type of cellular damage initiates a different mechanism for increasing cytoplasmic calcium (Shannon et al., 2017). In that report, we identified wound-induced microtears in the plasma membranes of surviving cells, and these microtears provided an entry for extracellular calcium to flood into the cytoplasm and then flow out to neighboring undamaged cells via gap junctions. This direct entry of calcium through damaged plasma membranes is evident within milliseconds after wounding. In this report we describe a second mechanism that extends to more distal cells, initiated by cell lysis at wounding. The dynamics of protease release from lysed cells, along with the gradual accumulation of active Gbp and its rapid diffusion, all contribute to the appearance of this distal calcium response 45-75 s after wounding. The earliest and closest cells to be activated by Mthl10/Gbp signaling cannot be identified visually because the initial flood of calcium through microtears takes time to subside.

Three tools allowed us to decipher these superimposed mechanisms. The first tool was the laser itself, which generates a highly stereotyped pattern of damage within a circular wound bed. Although cell lysis and plasma membrane damage are features of nearly every wound, their reproducible pattern in a laser wound allowed us to distinguish the signaling mechanisms each type of damage potentiated. The second tool was a spatio-temporal

analytical framework to measure radius over time, which clearly identified two peaks, the first induced by microtears and the second induced by cell lysis. The third tool was experimental, using RNAi-knock down of genes in a limited region and comparing it with an internal control. The ability to identify asymmetry between the control and experimental sides of wounds allowed us to bypass concerns about variable wound sizes, which otherwise would have made it difficult to recognize patterns and interpret data. Complex overlapping patterns may have obscured the mechanisms upstream of wound-induced calcium in other systems as well as ours.

Other upstream regulators of wound-induced calcium

Previous studies identified other molecules and phenomena upstream of wound-induced calcium. Studies in cell culture found that wound-generated cell lysis releases ATP, which diffuses extracellularly to bind to purinergic receptors and activate calcium release from intracellular stores (Arcuino et al., 2002; Boucher et al., 2010; Enyedi and Niethammer, 2015; Gault et al., 2014; Sieger et al., 2012; Weinger et al., 2005). Although reproducible in many types of cultured cells, there has been little evidence to support ATP signaling from lytic cells *in vivo*, likely because extracellular ATP is rapidly hydrolyzed by nucleotidases *in vivo* (Zimmermann et al., 2012). Interestingly, ATP does appear to signal damage and promote motility in response to injuries associated with cell swelling in zebrafish, animals that inhabit a hypotonic aqueous environment; however, even in this wounding paradigm, ATP does not signal from lytic cells at an appreciable level (Gault et al., 2014). We did not find evidence for ATP signaling upstream of calcium in our wounding experiments, as knockdown of the only fly adenosine receptor did not alter the calcium pattern around wounds.

Some *in vivo* studies have implicated a TrpM ion channel upstream of calcium release. This role of TrpM was first identified in laser-wounding studies of the *C. elegans* hypodermis (Xu and Chisholm, 2011), a giant syncytial cell where we would expect great overlap in the spatial extent of microtear-initiated calcium, which would diffuse quickly throughout a syncytium, and receptor-mediated calcium released from the ER. In the hypodermis, loss of TrpM reduced by half the intensity of wound-induced calcium signaling, but without spatial and temporal analysis, the exact contribution of TrpM is not known. In the *Drosophila* notum, a previous study identified TrpM as a regulator of wound-induced actin remodeling, and a slight reduction in wound-induced calcium intensity over time was noted in *TrpM* knockdowns (Antunes et al., 2013). In contrast, we did not observe any change in the spatial or temporal aspects of the calcium response in *TrpM* knockdown cells compared to the internal control, and given wound-to-wound variability it would have been hard to identify a small effect without an internal control. A study in the fly embryo determined that wound-induced calcium originates from both the external environment and internal stores (Razzell et al., 2013), suggesting to us that two superimposed calcium response mechanisms may have been at play in these experiments. They found when *TrpM* was knocked down, calcium intensity was reduced by half, but again without spatial and temporal analysis or an internal control, it is difficult to know what pathway TrpM regulates.

Tissue mechanics are upstream of increases in cytoplasmic calcium in a non-wounding context. Several labs have reported calcium flashes and waves in unwounded wing discs, dissected from larvae and cultured *ex vivo* (Balaji et al., 2017; Narciso et al., 2015; Restrepo and Basler, 2016). Cell and organ culture requires serum to support metabolism outside the organism, and in fly culture, this "serum" is generated by grinding whole adult flies and collecting the supernatant. Because such serum would undoubtedly contain secreted signals from wounded cells, calcium signaling in wing discs *ex vivo* is probably a wound response; indeed, we found it to be transduced by the same mechanism as wound signals, requiring protease, Gbps, and Mthl10. One aspect of calcium signaling in wing discs that we have not tested in our wounding model, however, is the role of mechanical tension. In carefully controlled mechanical experiments, fly serum was found to induce calcium flashes in wing discs specifically on the release of mechanical compression, indicating that tension is a requirement for calcium signaling in these wing discs (Narciso et al., 2017). It is interesting to consider the TrpM results in light of these mechanical studies, as some TrpM channels can be mechanosensitive. Together, these data suggest that there may be a role for mechanical tension in wound-induced calcium responses.

Functions of the Gbp/Mthl10 induced calcium increase around wounds.

We have found two independent mechanisms that increase cytoplasmic calcium, and in the cells at the wound margin these mechanisms would appear to act redundantly. Such redundancy indicates that the role of calcium in these cells is very important for wound healing. One biological pathway that may be downstream of calcium in these cells is recruitment of actin and myosin to the wound margin (Antunes et al., 2013; Bement et al., 1999; Wales et al., 2016) to form an actomyosin purse-string that cinches the wound closed (Antunes et al., 2013;Bement et al., 1999; Wood et al., 2002). What about calcium in the distal cells, regulated by Gbp/Mthl10? There are many possible functions, but at the moment, all of them are speculative. One possibility is that the cytosolic calcium response initiates distal epithelial cells to modify their cellular behavior from a stationary/non-proliferative state to a migratory and/or proliferative state necessary to repair the wound. Alternatively, an increase in cytosolic calcium may act to modulate an inflammatory response through DUOX leading to the formation of hydrogen peroxide to recruit inflammatory cells to the wound (Razzell et al., 2013) or through the calcium-dependent activation of cytoplasmic Phospholipase A_2 leading to the rapid recruitment of immune cells to tissue damage (Enyedi et al., 2016). This possibility is intriguing because Gbp is known to activate an immune response leading to the upregulation of antimicrobial peptides (Tsuzuki et al., 2012) and to increased activity of phagocytic plasmatocytes in a calcium-dependent manner (Tsuzuki et al., 2014). Interestingly, loss of Methuselah-like (Mthl) GPCRs results in increased lifespans (Cvejic et al., 2004; Lin et al., 1998; Sung et al., 2017), and Gbps are nutrition-sensitive peptides whose expression is reduced under starvation conditions (Koyama and Mirth, 2016). Increased lifespan, caloric restriction and decreased inflammation have all been linked (Franceschi et al., 2017; Gredilla and Barja, 2005; McCay et al., 1935; Zeng et al., 2016), and Gbp/Mthl10 activation at wounds may be part of this link.

Although the cytokine and GPCR families are widely conserved, Gbp and Mthl10 do not have direct orthologs in chordates. Nonetheless, similarities exist between the Gbp/Mthl10 mechanism and wound responses in other organisms. Damage- or pathogen-induced activation of proteins by proteolytic cleavage has been well documented in the cases of spätzle in the Toll pathway (Chasan et al., 1992; Morisato and Anderson, 1994; Valanne et al., 2011), thrombin and fibrin in the blood coagulation pathway (Macfarlane, 1969; Schmidt, 1872; Torbet, 1995), and IL-1β and IL-18 in the pyroptosis pathway (Bergsbaken et al., 2009; Fantuzzi and Dinarello, 1999; Fink and Cookson, 2005). Additionally, wound-defense signaling in plants relies on an immunomodulatory plant elicitor peptide that is cleaved into its active form by cysteine proteases upon damage-induced cytosolic calcium (Hander et al., 2019), and the plant defense hormone systemin is cleaved into its active form by phytaspases in response to damage or predation (Beloshistov et al., 2018). Because the basic circuitry is similar across kingdoms, our study suggests an ancient strategy for wound detection based on proprotein cleavage, activated by proteases released via cell lysis. As these examples make clear, proteases are already known to play critical roles in blood clotting and immune signaling, and this study finds that proteases are also instructive signals in epithelial wound detection.

Limitations of the Study

As noted above, the Gbp ligands and Mthl10 receptor are not present in mammals, so the extent of mechanistic conservation is unclear. Further, we have not experimentally tested this wound-detection mechanism in other developmental stages of *Drosophila*. For the computational model, several simplifications were made: the use of one variable for all proteases and one variable for all Gbps, rather than having separate Gbp1 and Gbp2; the use of simplified receptor/ligand dynamics that do not include uptake or recycling; and the use of a ligand-receptor binding threshold rather than inclusion of the signal transduction cascade between receptor-binding and calcium release. Finally, this study does not describe or address the mechanism behind the calcium flares that continue for at least an hour after wounding.

STAR Methods

RESOURCE AVAILABILITY

Lead contact—Further information and requests for resources and reagents should be directed to and will be fulfilled by the Lead Contact, Andrea Page-McCaw (andrea.page-mccaw@vanderbilt.edu)

Materials availability—Fly lines generated in this study are available from the Bloomington Drosophila Stock Center or from the Lead Contact.

Data and code availability—Code generated for the Reaction-Diffusion Model has been deposited on Github (https://doi.org/10.5281/zenodo.4977106).

EXPERIMENTAL MODEL AND SUBJECT DETAILS

Drosophila melanogaster—The *Drosophila* lines used for this study are detailed in Table S1. The complete genotype for each figure panel is provided in Table S2. *Drosophila* were maintained on standard cornmeal-molasses media supplemented with dry yeast. With the exception of flies containing *Gal80*^{TS}, flies were housed in plastic tubes in incubators between 18°C–25°C.

Fly crosses where the progeny will express Gal80^{TS} were maintained at 18°C for 2 days to inhibit Gal4 activation during embryogenesis. Progeny were then incubated at 29°C to activate Gal4, where they remained until experimentation. Thus, 3rd instar larvae were incubated at 29°C for 3-4 days before wing disc dissections and pupae were incubated at 29°C for 4-5 days before wounding.

***Drosophila* extract preparation—**Fly and larval extract was made following a protocol adapted from (Brodskiy et al., 2019) and (Currie et al., 1988). Briefly, 100 healthy adult flies with a female:male ratio of 3:1 or 100 healthy 3rd instar larvae, from non-overcrowded bottles, were homogenized in 750 µl of Schneider's *Drosophila* media (Thermo Fisher, #21720024). The resulting homogenates were centrifuged at 4°C for 20 minutes at 2600g. The supernatant was heat treated at 60°C for 5 minutes, before a second centrifugation at 4°C for 90 minutes at 2600*g*. The resulting supernatant – considered 100% extract – was aliquoted and stored at −20°C.

METHOD DETAILS

Pupal mounting—White prepupae were identified and aged for 12-18 hours After Puparium Formation (APF) at 29°C. Each pupa was placed ventral side down on a piece of double-sided tape (Scotch brand, catalog #665) adhered to a microscope slide, and the anterior pupal case was removed with fine tipped forceps to reveal the head and thorax (as in Fig. 1A, Shannon et al., 2017). The entire piece of double-sided tape (with dissected pupa) was gently lifted off the microscope slide and adhered to a 35 mm x 50 mm coverslip (Fisherbrand, cat#125485R) so the pupa is laid against the coverslip notum-side down, with the pupa sandwiched between the coverslip and the tape layer. Then, an oxygen permeable membrane (YSI, standard membrane kit, cat#1329882) was applied over the pupa and secured to the coverslip with additional double-sided tape so the pupa would not become dehydrated or deprived of oxygen.

Pupal survival—When mounted as described above, pupae developed normally for the next 3-4 days until eclosion, whereupon the adult flies crawled out of their cases and became stuck on the double-sided tape a few inches away. Pupal survival was measured as whether a pupa had developed into an adult fly and emerged from its case in this manner within 7 days after wounding (to ensure a pupa delayed in development was not accidentally miscounted as dead). Slides of pupae were returned to 29°C during this recovery phase after wounding to maintain Gal4 activation.

Live imaging—Live imaging of pupae was performed using a Zeiss (Oberkochen, Germany) LSM410 raster-scanning inverted confocal microscope with a 40X 1.3 NA oil-

immersion objective. Raster-scans were performed with a 2.26 s scan time per image with no interval between scans. Live imaging of wing discs was performed on the same scope, with the confocal settings turned off to maximize imaging depth, using a 25X 0.8 NA air objective. Raster-scans were performed with a 2.26 s scan time per image with a 15 s interval between scans. Notum picture in Fig. 1A' was taken on the same scope at 10X 0.50 NA air objective.

Images collected specifically for Fig. 7C–F were captured on a Nikon Ti2 Eclipse with X-light V2 spinning disc (Nikon, Tokyo, Japan) with a 40X 1.3 NA oil-immersion objective.

Laser ablation—Laser ablation was performed using single pulses of the 3rd harmonic (355 nm) of a Q-switched Nd:YAG laser (5 ns pulse-width, Continuum Minilite II, Santa Clara, CA). Laser pulse energies were on the order of 1 μJ, but were varied day to day and based on focal plane of ablation in order to optimize consistent wound sizes. A separate computer-controlled mirror and custom ImageJ plug-in were used to aim and operate the ablation laser so that ablation could be performed without any interruption to live imaging. The frame during ablation was retroactively considered t = 0 s.

Puncture wounding—Multiple pupae were placed on a piece of double-sided tape (Scotch brand, catalog #665), ventral side down on a microscope slide, and each anterior pupal case was removed with fine tipped forceps to reveal the notum epithelium (as in Fig. 1A). The slide was mounted on the stage of an upright epifluorescence microscope (Zeiss Axio M2) and imaged with a 1 s interval on a 5x objective (Zeiss EC Plan-NEOFLUAR 420330-9901). Pupae expressing GCaMP6m were manually punctured with an electrolytically sharpened tungsten needle (Fine Science Tools, No: 10130) while imaging. The frame when the puncture occurred was retroactively considered t = 0 s. Unfortunately, many puncture wounds resulted in a bubble of hemolymph that pooled over the wound, obscuring the initial influx and first expansion from multiple samples. However, the distal calcium response was always speckled in gap-junction knockdowns and always absent in G_q-pathway knockdowns, recapitulating laser wounds.

Wing disc mounting—Wing discs from 3rd instar larvae were dissected in Schneider's *Drosophila* media (Gibco, Life Technologies, Ref:21720-024) and immediately mounted in a small bubble of Schneider's *Drosophila* media on coverslips (Fisherbrand, cat#125485R) for imaging. A pap pen (RPI, catalog #50-550-221) was used to trace a hydrophobic barrier around the wing discs on the coverslip. Two wing discs, control and experimental, were mounted side-by-side in the same media bubble. The control disc was identifiable by the presence of mCherry which was not present in the experimental disc. Images were taken to establish a baseline of GCaMP fluorescence, and then potential calcium activators were pipetted directly into the media bubble over the wing discs. The concentration of calcium activators in the text refers to the final concentration after addition to the media bubble. The image taken during pipetting was retroactively considered t = 0 s.

Protease inhibition experiments—To test whether Δ*Gbp1,2* Larval Extract elicits a calcium response in control wing discs via proteases, we pre-mixed protease inhibitor cocktails or vehicle-only controls either into the extract or media bubble before addition

to the wing disc. Specifically, we used 1) Cell Signaling Technologies Protease inhibitor cocktail (Cell Signaling Technology, #5871S), which had no effect on the extract-mediated calcium response of Δ*Gbp1,2* Larval Extract when mixed at or below the 2x recommended concentration; at 3x recommended concentrations, the inhibitor itself elicited an ectopic calcium response on the discs, making it unusable for properly testing the extract-mediated calcium response. 2) MS-Safe Protease and Phosphatase inhibitor (Millipore Sigma, MSSAFE), which had no effect on the extract-mediated calcium response of Δ*Gbp1,2* Larval Extract when mixed at or below the 1x recommended concentration; at 1.5x recommended concentrations, the inhibitor itself elicited an ectopic calcium response on the discs, making it unusable for properly testing the extract-mediated calcium response. 3) Two other protease inhibitors tested (Millipore Sigma, 539134 and Millipore Sigma, 539133) used DMSO as a vehicle, which itself induces an ectopic calcium response in wing discs at even small concentrations (1% final v/v). Therefore, both of these protease inhibitors were not usable for properly testing the extract-mediated calcium response.

Peptide synthesis—The amino acid sequence for Growth-blocking peptides 1–5 is shown below (Tsuzuki et al., 2012).

Gbp1 (CG15917): ILLETTQKCKPGFELFGKRCRKPA

Gbp2 (CG11395): SLFNLDPKCAEGLKLMAGRCRKEA

Gbp3 (CG17244): MVAMIDFPCQPGYLPDHRGRCREIW

Gbp4 (CG12517): ILLDTSRKCRPGLELFGVRCRRRA

Gbp5 (CG14069): MLLEIQKRCWAGWGLLAGRCRKLA

These sequences were sent to Genscript (Piscataway, NJ. USA) for peptide synthesis under conditions to maintain the disulfide bond. The lyophilized peptide was reconstituted in ultrapure water, diluted to a concentration of 0.1 μM, aliquoted, and frozen at −80°C.

Protease preparation—Cysteine protease Clostripain (Alfa Aesar, Thermo Fisher, Stock: J61362) was reconstituted in a TBS solution (10 mM Tris, 1 mM $CaCl_2$, 50 mM NaCl, 2.5 mM beta-mercaptoethanol) to a final concentration of 1mg/mL (18.9 μM). This was aliquoted and frozen at −20°C. Serine protease trypsin (Gibco, Life Technologies, Ref: 25300-054) arrived at a concentration of 0.05% w/v (21.4 μM) and was refrigerated at 4°C.

ActinP-GCaMP6m* generation—pBPw.Act5CP-GCaMP6m* was generated from the GCaMP6m plasmid pGP-CMV-GCaMP6m (Addgene, originally in (Chen et al., 2013)) and the Actin5c promoter (Struhl and Basler, 1993). Importantly, this construct features the full 4.4 Kb genomic enhancer sequence for actin, containing all the regulatory elements to drive ubiquitous expression, rather than the more commonly used 2.6 Kb actin promoter sequence which is not highly expressed in the pupal notum. This 4.4 Kb promoter was obtained as a gift from Gary Struhl (Columbia University, New York, NY). The *pBPw.Act5CP-GCaMP6m* construct was injected by BestGene (Chino Hills, CA. USA) into *Drosophila* using PhiC31 integrase at the attP40 site at 25C6 on Chromosome 2, generating the *ActinP-GCaMP6m* fly line.

***Gbp1*$^{\Delta}$ generation—**The *Gbp1*$^{\Delta}$ null mutant was created by targeting two CRISPR-mediated double-stranded breaks to the *Gbp1* gene locus (www.crisprflydesign.org). The following gRNAs were chosen:

#1) ATTTGCTCCCATCATTTATC

#2) CGGAAAACGATGCAGAAAGC

gRNAs sequences with extensions to allow for BbsI digestion were synthesized as single-stranded DNA oligos and annealed to form overhangs, then ligated to a pCFD5 vector (Addgene, #73914) digested with BbsI (NEB, #R3539S). Both plasmids were sequence-verified then injected by BestGene (Chino Hills, CA. USA) into *vas-Cas9* expressing *Drosophila* embryos (Bloomington Stock 51324). *vas-Cas9* was crossed out of progeny and mutants were identified by PCR for the presence of a *Gbp1* deletion.

On sequencing, *Gbp1*$^{\Delta}$ was found to be missing 282 nucleotides, spanning the coding region corresponding to 94 amino acids from A22 to K116. This includes the C-terminal active peptide of the Gbp1 protein, which spans I95 to A118.

***Gbp2*$^{3\Delta FS}$ generation—**The *Gbp2*$^{3\Delta FS}$ null mutant was created by targeting two CRISPR-mediated double-stranded breaks in the *Gbp2* gene locus, using the protocol above. The following gRNAs were chosen:

#1) GAATATTCAACGCTGCCGTT

#2) AATTCCATACAACCGCGTCC

On sequencing, the *Gbp2*$^{3\Delta FS}$ allele was found to create multiple lesions: 8 missense mutations within the protein coding region generating the following amino acid substitutions: P41S, N42H, V51G, I61N, V94G, P150S, N192I, and S218P. Additionally, 3 small regions were deleted from the protein coding region: 30 nucleotides corresponding to Q236–Q246, 60 nucleotides corresponding to S252–T272, and 128 nucleotides corresponding to G284–R326. The last deletion induced a frameshift, creating multiple missense mutations and 4 stop codons in the final 391 nucleotides of the gene, thus preventing transcription of the region corresponding to the C-terminal active peptide of the Gbp2 protein, which spans S433 to A456.

Figure design—Figures were created in Affinity Designer (Serif (Europe) Ltd, West Bridgford, United Kingdom) and Inkscape (Inkscape.org).

QUANTIFICATION AND STATISTICAL ANALYSIS

Calcium signal intensity analysis—Fluorescence intensity of wing discs was measured using the Measure Stack plug-in in ImageJ. The region of interest was defined around the entire wing disc using the polygon selection tool. The mean fluorescence intensity for each disc was graphed in Microsoft Excel as a function of time, with 0 s corresponding to the frame when calcium activators were added to the wing disc media. The $\Delta F/F_0$ value for each experiment was defined as the disc's fluorescence intensity in the initial frame of the movie subtracted from the disc's maximum intensity, normalized to the initial frame intensity.

Calcium signal radius analysis—To quantify the spread of calcium signals from full-frame time-lapse images (Fig. S6A, A'), the ImageJ Radial Profile Angle Plot plug-in was used on each image to determine the average GCaMP6m intensity profile as a function of distance from the center of the wound (Fig. S6B, B'). A custom MATLAB script was then used to determine the distance from the wound at which the intensity dropped to half its maximum. This distance corresponds to the radius of the radially-averaged calcium wave and plotting radius for each video frame yields a graph of calcium signal expansion over time, which was graphed in Microsoft Excel (Fig. S6A').

The only exception to this applies to the analysis for Fig. 7D–F. Because these images were taken on a different scope, the custom MATLAB script was not optimized to determine radius vs time automatically, so these images were quantified by hand. Different control images were taken for this data-set than the controls in Figure 3, and this may explain any small discrepancies in spatial or temporal response values.

For all movies with an internal control, *pnr>mCherry.NLS* expression was used to define the experimental and control domains (as in Fig. 1B). The average calcium signal within each domain was measured separately. After plotting calcium radius with respect to time, the Δradius value for each sample was defined as the maximum value of the control domain calcium radius minus the calcium radius of the *pnr*-expressing experimental domain at the same time point (as shown in Fig. 1E').

For movies without an internal control, R_{Max} was defined as the maximum value of the calcium radius and R_{1st} as the value of the calcium radius at the first expansion local maximum. Duration of distal calcium response was defined by the duration the calcium response remained greater than R_{1st}. Movies cut off before the distal calcium response dipped below R_{1st} were excluded from duration analysis. Start time was defined as the time after wounding where the calcium radius value increased for at least three consecutive frames (excluding the first expansion increase). Movies where this never occurred were excluded from start time analysis.

Statistical analysis—All statistical analysis was performed in GraphPad Prism (San Diego, CA. USA). Δradius values for all samples of each genotype were graphed in Prism, and statistical analysis was performed by one-way ANOVA with multiple comparisons of each genotype from Fig. 1, Fig. S1 and Fig. 2 simultaneously with respect to the control group from Fig. 1I. Values for radius, duration, and start time analyses in Fig. 3G–I and Fig. 7D–F were graphed in Prism and statistical analysis was performed by one-way ANOVA with multiple comparisons with respect to the control group. Similarly, $\Delta F/F_0$ values for all wing disc experiments were graphed in Prism, and statistical analysis was performed by Student's t-test in all cases except for Fig. 5C which was analyzed by two-way ANOVA with multiple comparisons of each genotype with respect to the control extract + control disc group. Each scatterplot displays the value for each sample as a point, with bars representing mean and SEM.

Supplementary Material

Refer to Web version on PubMed Central for supplementary material.

Acknowledgements

We thank E. Baehrecke (University of Massachusetts Medical School, Worcester, MA) for providing the *UAS-IP*$_3$ sponge fly stock; T. Koyama (IGC, Lisbon, Portugal) for providing the Δ*Gbp1,2* fly stock; the Bloomington *Drosophila* Stock Center (Bloomington, IN) and the National Institute of Genetics (Shizuoka, Japan) for *Drosophila* stocks; G. Struhl (Columbia University, New York, NY) for providing the plasmid containing the *Actin5c* promoter; G. Neuert, M. Tyska, J. Nordman, and I. Macara (Vanderbilt University, Nashville TN) for comments on the manuscript. Funding: This work was supported by the National Institute of General Medical Sciences (1R01GM130130 to A.P.M. and M.S.H.), the National Institute of Arthritis and Musculoskeletal and Skin Diseases (R21AR072510 to A.P.M.). E.K.S. was supported by the National Institute of Cancer (5T32CA119925) and J.O.C. was supported by the National Institute of Child Health and Human Development (T32HD007502) and the American Heart Association (19PRE34410069 to J.O.C.).

References

Antunes M, Pereira T, Cordeiro JV, Almeida L, and Jacinto A (2013). Coordinated waves of actomyosin flow and apical cell constriction immediately after wounding. The Journal of Cell Biology 202, 365–379. [PubMed: 23878279]

Arcuino G, Lin JH-C, Takano T, Liu C, Jiang L, Gao Q, Kang J, and Nedergaard M (2002). Intercellular calcium signaling mediated by point-source burst release of ATP. Proc National Acad Sci 99, 9840–9845.

Balaji R, Bielmeier C, Harz H, Bates J, Stadler C, Hildebrand A, and Classen A-K (2017). Calcium spikes, waves and oscillations in a large, patterned epithelial tissue. Scientific Reports 7, 42786–14. [PubMed: 28218282]

Beloshistov RE, Dreizler K, Galiullina RA, Tuzhikov AI, Serebryakova MV, Reichardt S, Shaw J, Taliansky ME, Pfannstiel J, Chichkova NV, et al. (2018). Phytaspase - mediated precursor processing and maturation of the wound hormone systemin. New Phytol 218, 1167–1178. [PubMed: 28407256]

Bement WM, Mandato CA, and Kirsch MN (1999). Wound-induced assembly and closure of an actomyosin purse string in Xenopus oocytes. Curr Biol 9, 579–587. [PubMed: 10359696]

Benink HA, and Bement WM (2005). Concentric zones of active RhoA and Cdc42 around single cell wounds. The Journal of Cell Biology 168, 429–439. [PubMed: 15684032]

Bergsbaken T, Fink SL, and Cookson BT (2009). Pyroptosis: host cell death and inflammation. Nature Reviews. Microbiology 7, 99–109. [PubMed: 19148178]

Boucher I, Rich C, Lee A, Marcincin M, and Trinkaus-Randall V (2010). The P2Y2 receptor mediates the epithelial injury response and cell migration. Am J Physiol-Cell Ph 299, C411–C421.

Brodskiy PA, Wu Q, Soundarrajan DK, Huizar FJ, Chen J, Liang P, Narciso C, Levis MK, Arredondo-Walsh N, Chen DZ, et al. (2019). Decoding Calcium Signaling Dynamics during Drosophila Wing Disc Development. Biophysical Journal 116, 725–740. [PubMed: 30704858]

Chang-Graham AL, Perry JL, Engevik MA, Engevik KA, Scribano FJ, Gebert JT, Danhof HA, Nelson JC, Kellen JS, Strtak AC, et al. (2020). Rotavirus induces intercellular calcium waves through ADP signaling. Science (New York, N.Y.) 370, eabc3621.

Chasan R, Jin Y, and Anderson KV (1992). Activation of the easter zymogen is regulated by five other genes to define dorsal-ventral polarity in the Drosophila embryo. Development 115, 607–616. [PubMed: 1425342]

Chen T-W, Wardill TJ, Sun Y, Pulver SR, Renninger SL, Baohan A, Schreiter ER, Kerr RA, Orger MB, Jayaraman V, et al. (2013). Ultrasensitive fluorescent proteins for imaging neuronal activity. Nature 499, 295–300. [PubMed: 23868258]

Currie DA, Milner MJ, and Evans CW (1988). The growth and differentiation in vitro of leg and wing imaginal disc cells from Drosophila melanogaster. Development 102, 805.

Cvejic S, Zhu Z, Felice SJ, Berman Y, and Huang X-Y (2004). The endogenous ligand Stunted of the GPCR Methuselah extends lifespan in Drosophila. Nat Cell Biol 6, 540–546. [PubMed: 15133470]

D'hondt C, Himpens B, and Bultynck G (2013). Mechanical stimulation-induced calcium wave propagation in cell monolayers: the example of bovine corneal endothelial cells. Journal of Visualized Experiments : JoVE e50443. [PubMed: 23892350]

Endo Y, Ohnishi A, and Hayakawa Y (1998). Mechanism of parasitism-induced elevation of haemolymph growth-blocking peptide levels in host insect larvae (Pseudaletia separata). Journal of Insect Physiology 44, 859–866. [PubMed: 12769880]

Enyedi B, and Niethammer P (2015). Mechanisms of epithelial wound detection. Trends Cell Biol 25, 398–407. [PubMed: 25813429]

Enyedi B, Jelcic M, and Niethammer P (2016). The Cell Nucleus Serves as a Mechanotransducer of Tissue Damage-Induced Inflammation. Cell 165, 1160–1170. [PubMed: 27203112]

Fantuzzi G, and Dinarello CA (1999). Interleukin-18 and interleukin-1 beta: two cytokine substrates for ICE (caspase-1). Journal of Clinical Immunology 19, 1–11. [PubMed: 10080100]

Fink SL, and Cookson BT (2005). Apoptosis, pyroptosis, and necrosis: mechanistic description of dead and dying eukaryotic cells. Infection and Immunity 73, 1907–1916. [PubMed: 15784530]

Franceschi C, Garagnani P, Vitale G, Capri M, and Salvioli S (2017). Inflammaging and 'Garb-aging.' Trends Endocrinol Metabolism 28, 199–212.

Frank D, and Vince JE (2019). Pyroptosis versus necroptosis: similarities, differences, and crosstalk. Cell Death Differ 26, 99–114. [PubMed: 30341423]

Gao K, Wang CR, Jiang F, Wong AYK, Su N, Jiang JH, Chai RC, Vatcher G, Teng J, Chen J, et al. (2013). Traumatic scratch injury in astrocytes triggers calcium influx to activate the JNK/c-Jun/AP-1 pathway and switch on GFAP expression. Glia 61, 2063–2077. [PubMed: 24123203]

Gasteiger E, Gattiker A, Hoogland C, Ivanyi I, Appel RD, and Bairoch A (2003). ExPASy: The proteomics server for indepth protein knowledge and analysis. Nucleic Acids Research 31, 3784–3788. [PubMed: 12824418]

Gault WJ, Enyedi B, and Niethammer P (2014). Osmotic surveillance mediates rapid wound closure through nucleotide release. J Cell Biol 207, 767–782. [PubMed: 25533845]

Gomes P, Malfait M, Himpens B, and Vereecke J (2003). Intercellular Ca(2+)-transient propagation in normal and high glucose solutions in rat retinal epithelial (RPE-J) cells during mechanical stimulation. Cell Calcium 34, 185–192. [PubMed: 12810061]

Gredilla R, and Barja G (2005). Minireview: The Role of Oxidative Stress in Relation to Caloric Restriction and Longevity. Endocrinology 146, 3713–3717. [PubMed: 15919745]

Guruharsha KG, Rual J-F, Zhai B, Mintseris J, Vaidya P, Vaidya N, Beekman C, Wong C, Rhee DY, Cenaj O, et al. (2011). A Protein Complex Network of Drosophila melanogaster. Cell 147, 690–703. [PubMed: 22036573]

Gutenkunst RN, Waterfall JJ, Casey FP, Brown KS, Myers CR, and Sethna JP (2007). Universally sloppy parameter sensitivities in systems biology models. PLoS Computational Biology 3, 1871–1878. [PubMed: 17922568]

Hander T, Fernández-Fernández ÁD, Kumpf RP, Willems P, Schatowitz H, Rombaut D, Staes A, Nolf J, Pottie R, Yao P, et al. (2019). Damage on plants activates Ca2+-dependent metacaspases for release of immunomodulatory peptides. Science (New York, N.Y.) 363, eaar7486.

Hanlon CD, and Andrew DJ (2015). Outside-in signaling--a brief review of GPCR signaling with a focus on the Drosophila GPCR family. Journal of Cell Science 128, 3533–3542. [PubMed: 26345366]

Hayakawa Y (1991). Structure of a growth-blocking peptide present in parasitized insect hemolymph. The Journal of Biological Chemistry 266, 7982–7984. [PubMed: 2022627]

Hunter MV, Lee DM, Harris TJC, and Fernandez-Gonzalez R (2015). Polarized E-cadherin endocytosis directs actomyosin remodeling during embryonic wound repair. The Journal of Cell Biology 210, 801–816. [PubMed: 26304727]

Hunter MV, Willoughby PM, Bruce AEE, and Fernandez-Gonzalez R (2018). Oxidative Stress Orchestrates Cell Polarity to Promote Embryonic Wound Healing. Developmental Cell 47, 377–387.e4. [PubMed: 30399336]

Klepeis VE, Cornell-Bell A, and Trinkaus-Randall V (2001). Growth factors but not gap junctions play a role in injuryinduced Ca2+ waves in epithelial cells. Journal of Cell Science 114, 4185–4195. [PubMed: 11739651]

Kong D, Lv Z, Häring M, Lin B, Wolf F, and Großhans J (2019). In vivo optochemical control of cell contractility at single-cell resolution. EMBO Reports 20, e47755. [PubMed: 31663248]

Koyama T, and Mirth CK (2016). Growth-Blocking Peptides As Nutrition-Sensitive Signals for Insulin Secretion and Body Size Regulation. PLoS Biology 14, e1002392. [PubMed: 26928023]

Lemon G, Gibson WG, and Bennett MR (2003). Metabotropic receptor activation, desensitization and sequestration-I: modelling calcium and inositol 1,4,5-trisphosphate dynamics following receptor activation. Journal of Theoretical Biology 223, 93–111. [PubMed: 12782119]

Levy HM, and Ryan EM (1965). Evidence that calcium activates the contraction of actomyosin by overcoming substrate inhibition. Nature 205, 703–705.

Lin Y-J, Seroude L, and Benzer S (1998). Extended Life-Span and Stress Resistance in the *Drosophila* Mutant *methuselah*. Science 282, 943–946. [PubMed: 9794765]

Macfarlane RG (1969). A. The blood clotting mechanism. The development of a theory of blood coagulation. Proceedings of the Royal Society of London. Series B, Biological Sciences 173, 261–268.

Martin P, and Lewis J (1992). Actin cables and epidermal movement in embryonic wound healing. Nature 360, 179–183. [PubMed: 1436096]

Matsumoto Y, Oda Y, Uryu M, and Hayakawa Y (2003). Insect cytokine growth-blocking peptide triggers a termination system of cellular immunity by inducing its binding protein. The Journal of Biological Chemistry 278, 38579–38585. [PubMed: 12871935]

McCay CM, Crowell MF, and Maynard LA (1935). The Effect of Retarded Growth Upon the Length of Life Span and Upon the Ultimate Body Size. J Nutrition 10, 63–79.

McNeil PL, and Steinhardt RA (2003). Plasma membrane disruption: repair, prevention, adaptation. Annual Review of Cell and Developmental Biology 19, 697–731.

Morisato D, and Anderson KV (1994). The spätzle gene encodes a component of the extracellular signaling pathway establishing the dorsal-ventral pattern of the Drosophila embryo. Cell 76, 677–688. [PubMed: 8124709]

Narciso C, Wu Q, Brodskiy P, Garston G, Baker R, Fletcher A, and Zartman J (2015). Patterning of wound-induced intercellular Ca(2+) flashes in a developing epithelium. Physical Biology 12, 056005. [PubMed: 26331891]

Narciso CE, Contento NM, Storey TJ, Hoelzle DJ, and Zartman JJ (2017). Release of Applied Mechanical Loading Stimulates Intercellular Calcium Waves in Drosophila Wing Discs. Biophysical Journal 113, 491–501. [PubMed: 28746859]

Port F, Chen H-M, Lee T, and Bullock SL (2014). Optimized CRISPR/Cas tools for efficient germline and somatic genome engineering in Drosophila. Proc National Acad Sci 111, E2967–E2976.

Razzell W, Evans IR, Martin P, and Wood W (2013). Calcium flashes orchestrate the wound inflammatory response through DUOX activation and hydrogen peroxide release. Current Biology : CB 23, 424–429. [PubMed: 23394834]

Restrepo S, and Basler K (2016). Drosophila wing imaginal discs respond to mechanical injury via slow InsP3R-mediated intercellular calcium waves. Nature Communications 7, 12450–12459.

Schindelin J, Arganda-Carreras I, Frise E, Kaynig V, Longair M, Pietzsch T, Preibisch S, Rueden C, Saalfeld S, Schmid B, et al. (2012). Fiji: an open-source platform for biological-image analysis. Nat Methods 9, 676–682. [PubMed: 22743772]

Schmidt A (1872). Neue Untersuchungen über die Faserstoffgerinnung. Archiv Für Die Gesamte Physiologie Des Menschen Und Der Tiere 6, 413–538.

Shabir S, and Southgate J (2008). Calcium signalling in wound-responsive normal human urothelial cell monolayers. Cell Calcium 44, 453–464. [PubMed: 18417211]

Shannon EK, Stevens A, Edrington W, Zhao Y, Jayasinghe AK, Page-McCaw A, and Hutson MS (2017). Multiple Mechanisms Drive Calcium Signal Dynamics around Laser-Induced Epithelial Wounds. Biophysical Journal 113, 1623–1635. [PubMed: 28978452]

Shears SB, and Hayakawa Y (2019). Functional Multiplicity of an Insect Cytokine Family Assists Defense Against Environmental Stress. Frontiers in Physiology 10, 222. [PubMed: 30967784]

Sieger D, Moritz C, Ziegenhals T, Prykhozhij S, and Peri F (2012). Long-Range Ca2+ Waves Transmit Brain-Damage Signals to Microglia. Dev Cell 22, 1138–1148. [PubMed: 22632801]

Skinner ME, Uzilov AV, Stein LD, Mungall CJ, and Holmes IH (2009). JBrowse: A next-generation genome browser. Genome Res 19, 1630–1638. [PubMed: 19570905]

Stanisstreet M (1982). Calcium and wound healing in Xenopus early embryos. Journal of Embryology and Experimental Morphology 67, 195–205. [PubMed: 6806425]

Struhl G, and Basler K (1993). Organizing activity of wingless protein in Drosophila. Cell 72, 527–540. [PubMed: 8440019]

Sung EJ, Ryuda M, Matsumoto H, Uryu O, Ochiai M, Cook ME, Yi NY, Wang H, Putney JW, Bird GS, et al. (2017). Cytokine signaling through Drosophila Mthl10 ties lifespan to environmental stress. Proceedings of the National Academy of Sciences of the United States of America 114, 13786–13791. [PubMed: 29229844]

Thuma L, Carter D, Weavers H, and Martin P (2018). Drosophila immune cells extravasate from vessels to wounds using Tre1 GPCR and Rho signaling. The Journal of Cell Biology 217, 3045–3056. [PubMed: 29941473]

Torbet J (1995). The thrombin activation pathway modulates the assembly, structure and lysis of human plasma clots in vitro. Thrombosis and Haemostasis 73, 785–792. [PubMed: 7482404]

Tsuzuki S, Ochiai M, Matsumoto H, Kurata S, Ohnishi A, and Hayakawa Y (2012). Drosophila growth-blocking peptidelike factor mediates acute immune reactions during infectious and non-infectious stress. Scientific Reports 2, 210–10. [PubMed: 22355724]

Tsuzuki S, Matsumoto H, Furihata S, Ryuda M, Tanaka H, Sung EJ, Bird GS, Zhou Y, Shears SB, and Hayakawa Y (2014). Switching between humoral and cellular immune responses in Drosophila is guided by the cytokine GBP. Nat Commun 5, 4628. [PubMed: 25130174]

Tu C-L, Celli A, Mauro T, and Chang W (2019). Calcium-Sensing Receptor Regulates Epidermal Intracellular Ca2+ Signaling and Re-Epithelialization after Wounding. The Journal of Investigative Dermatology 139, 919–929. [PubMed: 30404020]

Usui-Aoki K, Matsumoto K, Koganezawa M, Kohatsu S, Isono K, Matsubayashi H, Yamamoto M-T, Ueda R, Takahashi K, Saigo K, et al. (2005). Targeted expression of Ip3 sponge and Ip3 dsRNA impaires sugar taste sensation in Drosophila. Journal of Neurogenetics 19, 123–141. [PubMed: 16540404]

Valanne S, Wang J-H, and Rämet M (2011). The Drosophila Toll signaling pathway. Journal of Immunology (Baltimore, Md. : 1950) 186, 649–656.

Wales P, Schuberth CE, Aufschnaiter R, Fels J, García-Aguilar I, Janning A, Dlugos CP, Schäfer-Herte M, Klingner C, Wälte M, et al. (2016). Calcium-mediated actin reset (CaAR) mediates acute cell adaptations. ELife 5, 990.

Weinger I, Klepeis VE, and Trinkaus-Randall V (2005). Tri-nucleotide receptors play a critical role in epithelial cell wound repair. Purinergic Signalling 1, 281–292. [PubMed: 18404512]

Wood W, Jacinto A, Grose R, Woolner S, Gale J, Wilson C, and Martin P (2002). Wound healing recapitulates morphogenesis in Drosophila embryos. Nature Cell Biology 4, 907–912. [PubMed: 12402048]

Wu Y, Brock AR, Wang Y, Fujitani K, Ueda R, and Galko MJ (2009). A blood-borne PDGF/VEGF-like ligand initiates wound-induced epidermal cell migration in Drosophila larvae. Current Biology : CB 19, 1473–1477. [PubMed: 19646875]

Xu S, and Chisholm AD (2011). A Gαq-Ca^{2+} signaling pathway promotes actin-mediated epidermal wound closure in C. elegans. Current Biology : CB 21, 1960–1967. [PubMed: 22100061]

Yang L, Di G, Qi X, Qu M, Wang Y, Duan H, Danielson P, Xie L, and Zhou Q (2014). Substance P promotes diabetic corneal epithelial wound healing through molecular mechanisms mediated via the neurokinin-1 receptor. Diabetes 63, 4262–4274. [PubMed: 25008176]

Yoo SK, Freisinger CM, LeBert DC, and Huttenlocher A (2012). Early redox, Src family kinase, and calcium signaling integrate wound responses and tissue regeneration in zebrafish. The Journal of Cell Biology 199, 225–234. [PubMed: 23045550]

Zeng Y, Nie C, Min J, Liu X, Li M, Chen H, Xu H, Wang M, Ni T, Li Y, et al. (2016). Novel loci and pathways significantly associated with longevity. Sci Rep-Uk 6, 21243.

Zimmermann H, Zebisch M, and Sträter N (2012). Cellular function and molecular structure of ecto-nucleotidases. Purinerg Signal 8, 437–502.

Highlights

- Wounds induce a rapid increase in cytosolic calcium in cells around the wound
- The GPCR Mthl10 and its cytokine ligands Gbp1 and Gbp2 are required for this process
- Wound-induced proteases initiate the process by activating the cytokine proligands
- Computational modeling validates these steps as a mechanism for rapid wound detection

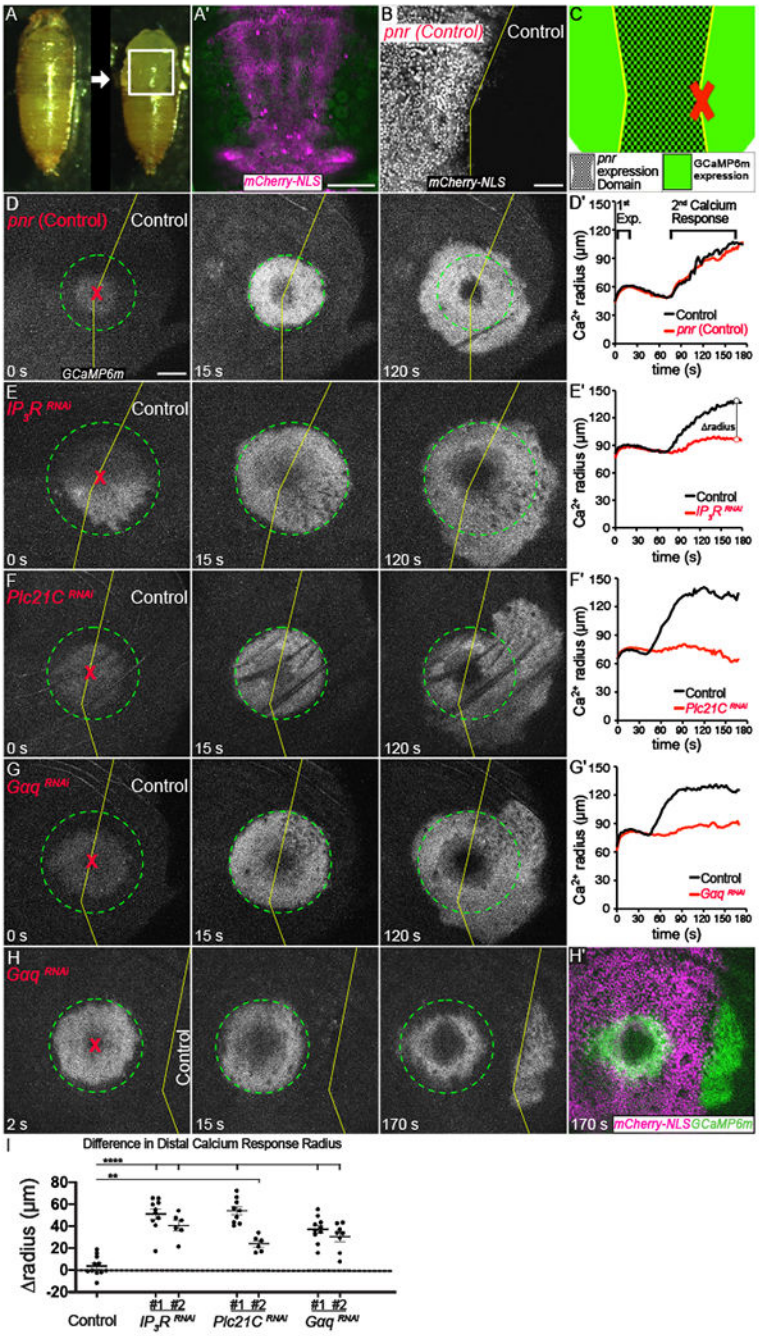

Figure 1. Wounds trigger calcium release via the G_q pathway.

(A) Experimental model, *Drosophila* pupa (left) with pupal case removed (right). Gene expression is controlled in the *pnr* domain, as delineated by mCherry-NLS (magenta in **A'**, grayscale in **B**). **(B-C)** wounds (red X) are targeted at the *pnr* boundary (yellow line, **B, C**). **(D-H)** GCaMP6m calcium reporter. **(D, D')** Calcium response to wounds in the absence of gene knock-down. The max radius of the rapid first calcium expansion is marked by green circle; the distal calcium response begins ~45-75 s after wounding. Analysis of the calcium radius with respect to time **(D')** demonstrates that the response is symmetric on both

sides of the *pnr* boundary, n = 11. **(E-G)** The distal calcium response requires G_q-pathway components knocked down on the left side *(pnr* domain) of each panel. *IP3R RNAi #1* n = 10, *IP3R RNAi* #2 n = 6, *PLC21C RNAi #1* n = 9, *PLC21C RNAi #1* n = 6, *Gαq RNAi #1* n = 10, *Gαq RNAi* #2 n = 8. (**D'**–**G'**) Quantification of calcium dynamics for control (black) and *pnr* (red) sides of wounds. **(H)** Wound targeted within the *Gαq* knock-down domain (left of yellow line) yields no distal calcium response until the initiating signal reaches the nearby control domain. (*H'*) Green shows calcium (*GCaMP6m*), magenta shows *pnr* domain where *Gαq* is knocked down. (**I**) Δradius, difference in calcium signal radii at maximum extent of the distal calcium response for control minus *pnr* side of each wound (as shown in E'), with *pnr*-knockdown genotypes indicated; bars = mean ± SEM. Statistical analysis by one-way ANOVA, which included all genotypes from Fig. 1, Fig. 2, and Fig. S1, multiple comparisons WRT control group, **p<0.01, ****p<0.0001. Scale bars = 200 μm (A'), or 50 μm (B-H'). See also: Figure S1, Movies 1–4.

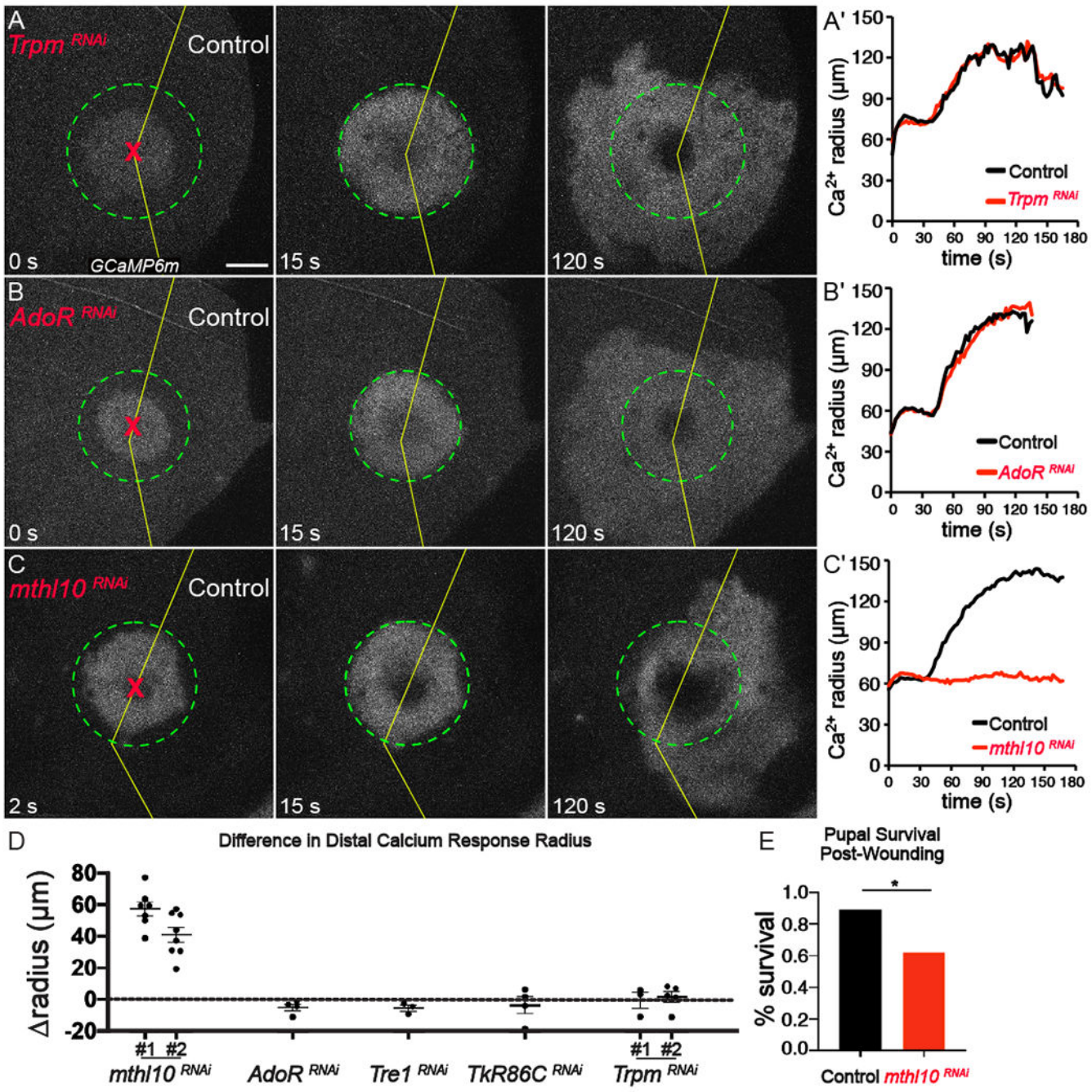

Figure 2: The distal calcium response requires the GPCR Methuselah-like 10 (Mthl10).

(A-C) GCaMP6m reporter showing cytosolic calcium in representative samples. RNAi of the indicated gene is limited to the *pnr* domain (left side), and wounds (red X) are administered at the *pnr* domain boundary (yellow line). Maximum extent of first expansion is marked by dashed green circle. (**A**) Knockdown of the calcium ion channel *TRPM* has no effect on either calcium response. *TRPM RNAi #1* n = 3, *TRPM RNAi* #2 n = 5 (**B**) Knockdown of the GPCR Adenosine Receptor (*AdoR*) has no effect on either calcium response. *AdoR RNAi* n = 4. (**C**) Knockdown of the GPCR *Methuselah-like 10* (*Mthl10*)

phenocopies the G_q-pathway knockdowns, with a dramatic decrease in the distal calcium response. *mthl10 RNAi #1* n = 7, *mthl10 RNAi* #2 n = 8. (**A'–C'**) Quantification of calcium signal radius versus time in control (black) and *pnr*-expression (red) sides of each wound. (**D**) Δradius between control and *pnr* sides, with *pnr*-knockdown genotypes indicated; bars = mean ± SEM. *Tre1 RNAi* n = 3, *TkR86C RNAi* n = 4. Both mthHO RNAi lines were statistically significant (****p<0.0001) by one-way ANOVA, which included all genotypes from Fig. 1, Fig. 2, and Fig. S1, multiple comparisons WRT control group from Fig. 1. (**E**) Pupal survival to adulthood after large wounds. Quantification by Chi-Square, n=29 each, p=0.0141. Scale bar= 50 μm. See also: Movie 5.

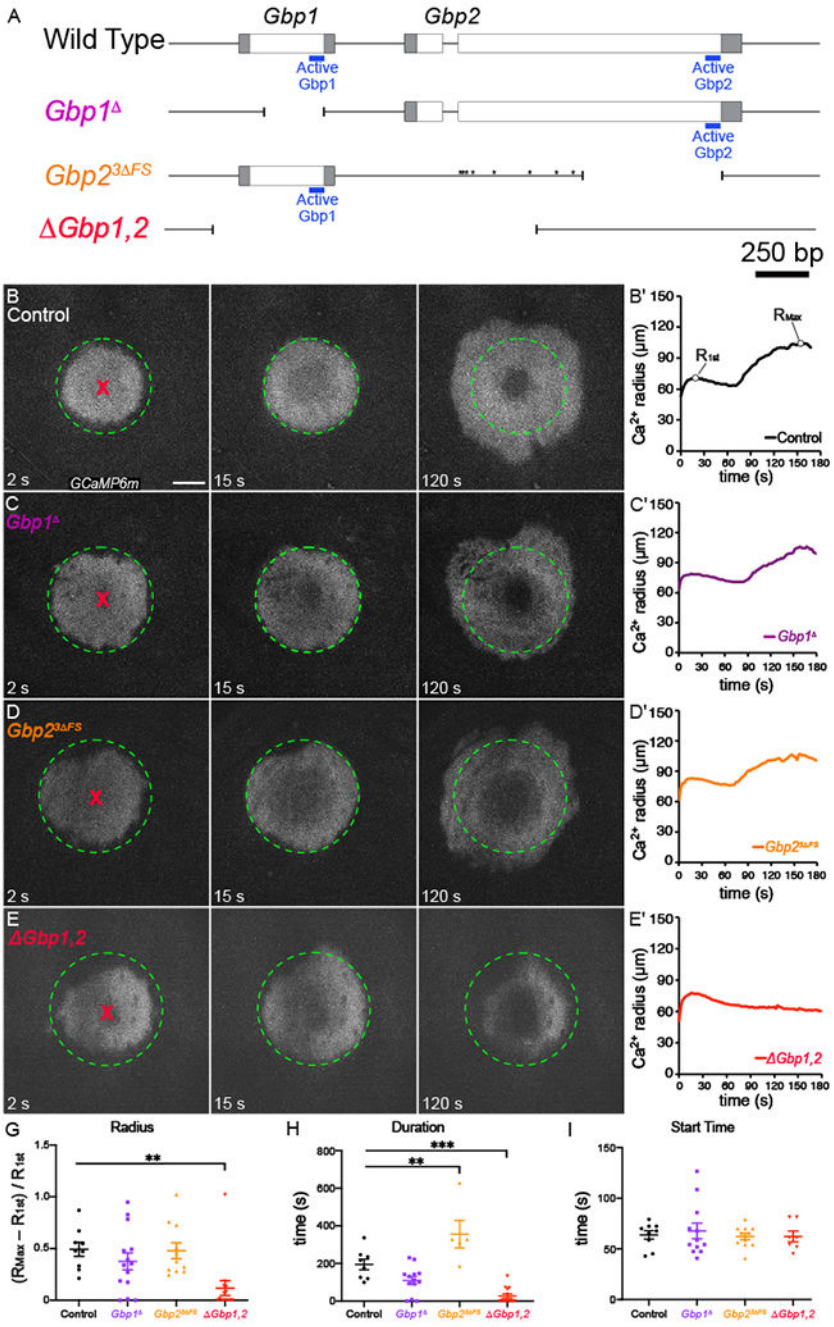

Figure 3: The distal calcium response requires either Gbp1 or Gbp2.

(**A**) Schematic showing the genomic region for *Gbp1* and *Gbp2*, the deletion Δ*Gbp1,2*, and the *Gbp1* or *Gbp2* null mutants generated for this study (transcription proceeds from left to right). The $Gbp1^{\Delta}$ deletion allele is missing 282 bases within the coding region of *Gbp1*, removing most of the region encoding the Gbp1 active peptide (blue). The complex $Gbp2^{3\Delta FS}$ allele comprises 8 point mutations (asterisks) and 3 deletions, inducing frameshifts and premature terminations upstream of the Gbp2 active peptide (blue) (see Methods). (**B-E**) GCaMP6m reporter showing cytosolic calcium in representative samples

of control or deletion mutants. Scale bar = 50 μm. (**B, B'**) The normal calcium response is present in controls (n = 9). (**C-D**) Homozygous *Gbp1*$^{\Delta}$ (**C**) or Gbp2$^{3\Delta FS}$ (**D**) each retain the distal calcium response (n = 14 and 11 respectively). (**E,E'**) A normal distal calcium response is absent after wounding homozygous Δ*Gbp1,2* in n=13/14. (**G**) Spatial quantification of each sample's maximum radius (R_{Max} in **B'**) normalized to its first expansion maximum radius (R_{1st} in **B'**). Δ*Gbp1,2* has a significantly decreased response compared to control, while the *Gbp1*$^{\Delta}$ and Gbp2$^{3\Delta FS}$ do not. (**H**) Duration that distal calcium response radius exceeded R_{1st}. Δ*Gbp1,2* has a significantly decreased duration compared to control, while surprisingly, *Gbp2*$^{3\Delta FS}$ was significantly increased. Movies cut off before the distal calcium response dipped below R_{1st} were excluded from **H**. (**I**) The start time, defined as the time when the calcium radius began consistently increasing for the distal calcium response, shows no significant differences. Samples where $R_{Max} = R_{1st}$ were excluded from **I**. Statistical analysis by one-way ANOVA, multiple comparisons WRT control group, **p<0.01, ***p<0.001.

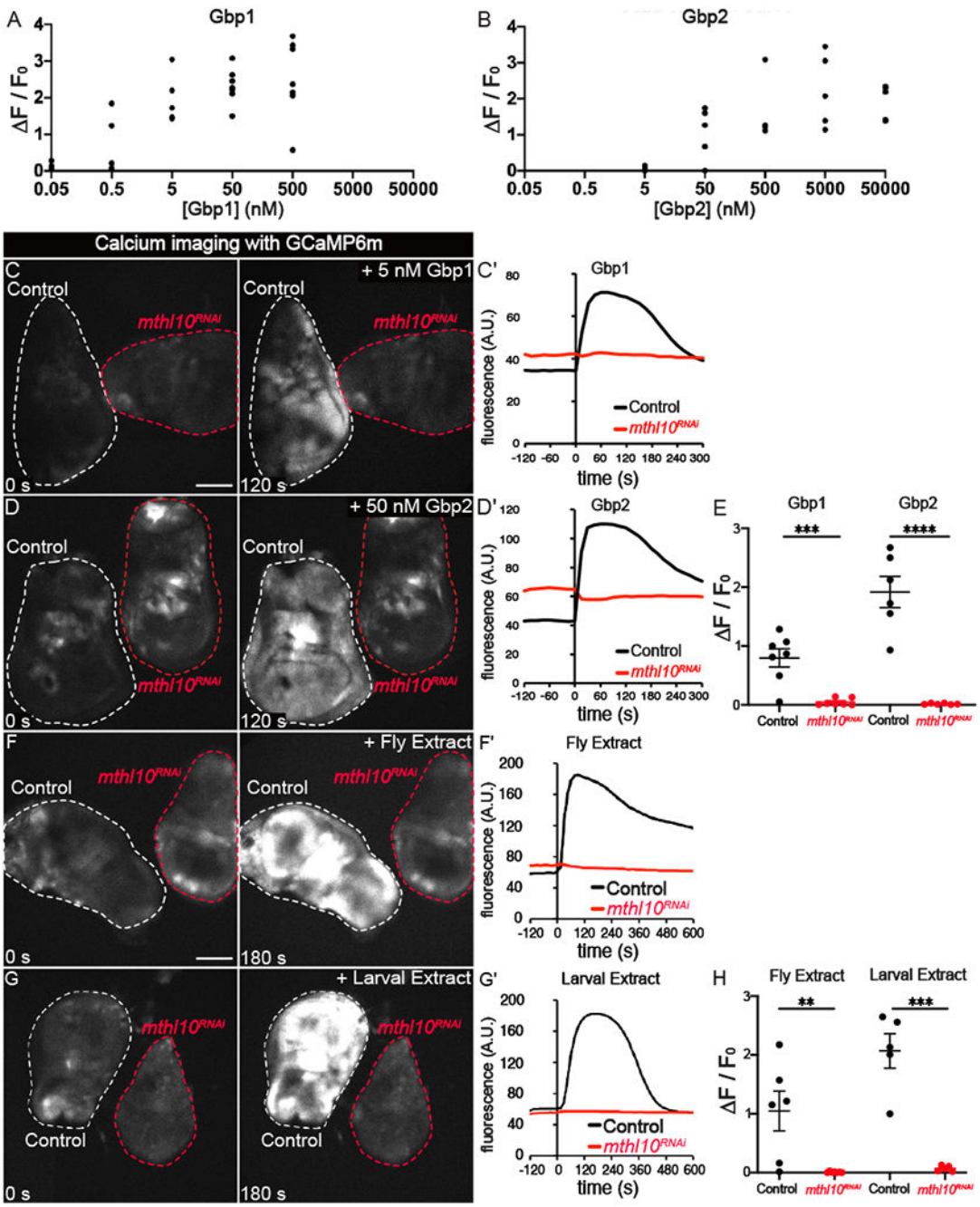

Figure 4: Gbp peptides and *Drosophila* extracts elicit calcium responses in wing discs through Mthl10.

(**A-B**) Gbp1 or Gbp2 peptides elicit a concentration-dependent calcium response in wing discs. Gbp1 additions n = 29, Gbp2 additions n = 21. 5 nM Gbp1 or 50 nM Gbp2 consistently elicits a calcium response. (**C-D, F-G**) Assays were performed with two wing discs (one control and one *mthl10* knockdown) mounted adjacently and activated simultaneously. *Mthl10* is required in wing discs for Gbp1 (**C**, n = 7) or Gbp2 (**D**, n = 6) to activate a calcium response. Change in GCaMP6m fluorescence over time for samples **C**

and **D** is quantified in **C'** and **D'**, respectively. (**E**) Normalized change in fluorescence is quantified for all samples. (**F-G**) *Mthl10* is required in wing discs for 5% fly extract (**F**, n = 6) or 5% larval extract (**G**, n = 5) to activate a calcium response. Change in GCaMP6m fluorescence over time for samples **F** and **G** is quantified in **F'** and **G'**, respectively. (**H**) Normalized change in fluorescence is quantified for all samples in **F'** and **G'**. Scale bar= 100 μm. Graph bars represent mean and SEM. **p<0.01, ***p<0.001, ****p<0.0001 by Student's t-test. See also: Figure S2, Movie 6–7.

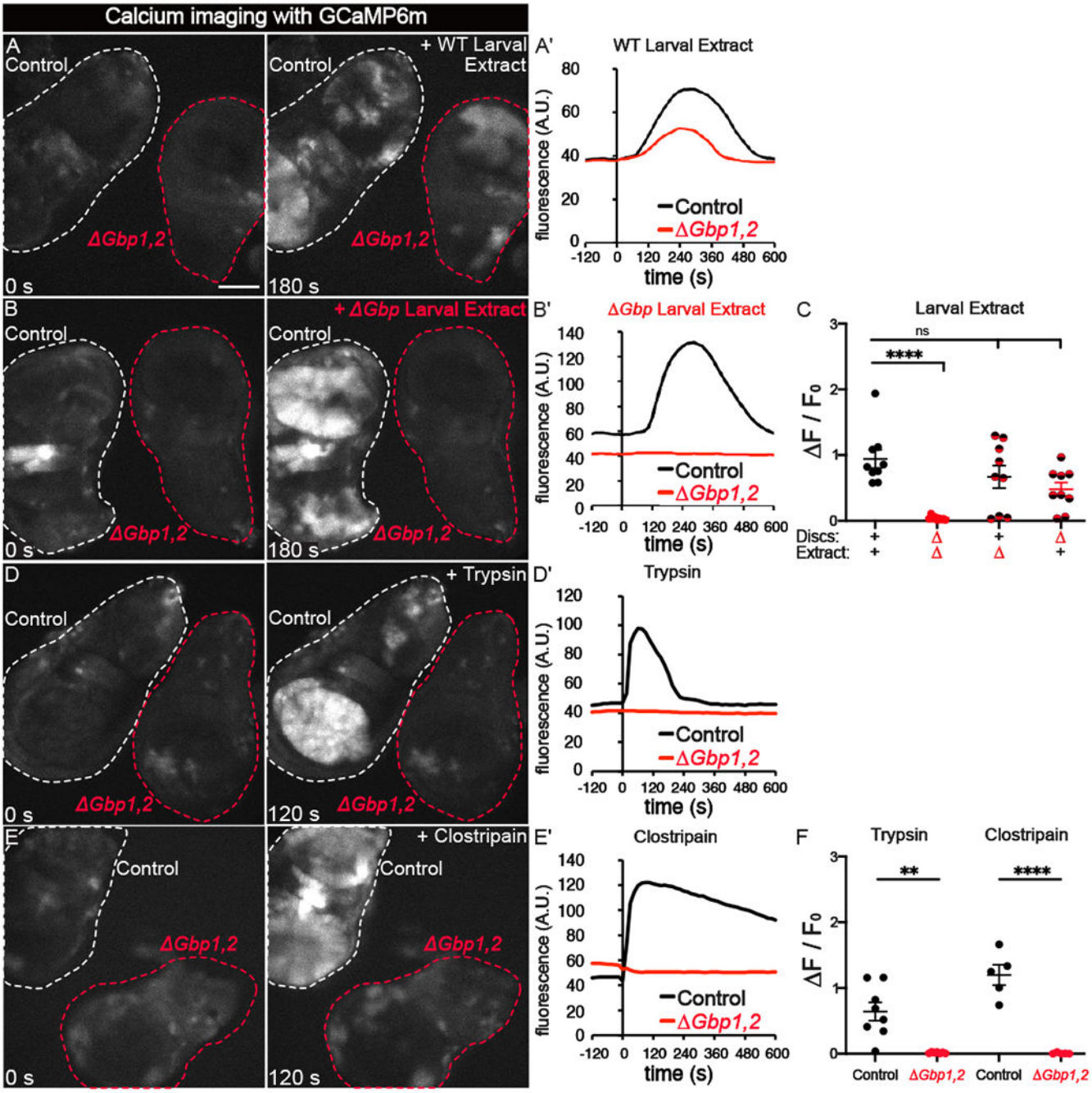

Figure 5: *Drosophila* extract and proteases require Gbps to elicit calcium responses.

(**A-F**) All assays were performed with two wing discs (one control and one Δ*Gbp1,2)* mounted adjacently and activated simultaneously. Scale bar =100 μm. (**A-C**) Gbp is required for the larval extract-mediated calcium response, as no response occurs if Gbp is absent from both extract and wing disc (**A, A'**, n = 9). The signal can be supplied by either the wing disc (**A, A'**) or by the larval extract (**B, B'**, n = 9). Normalized change in fluorescence is quantified in **C**. **(D-F)** Serine protease trypsin (**D**, n = 8) or cysteine protease clostripain (**E**, n = 5) activate calcium in a Gbp-dependent manner. Normalized change in fluorescence is

quantified in **F**. Graph bars represent mean and SEM. **p<0.01, ****p<0.0001 by two-way ANOVA in **C** and Student's t-test in **F**. See also: Movie 8.

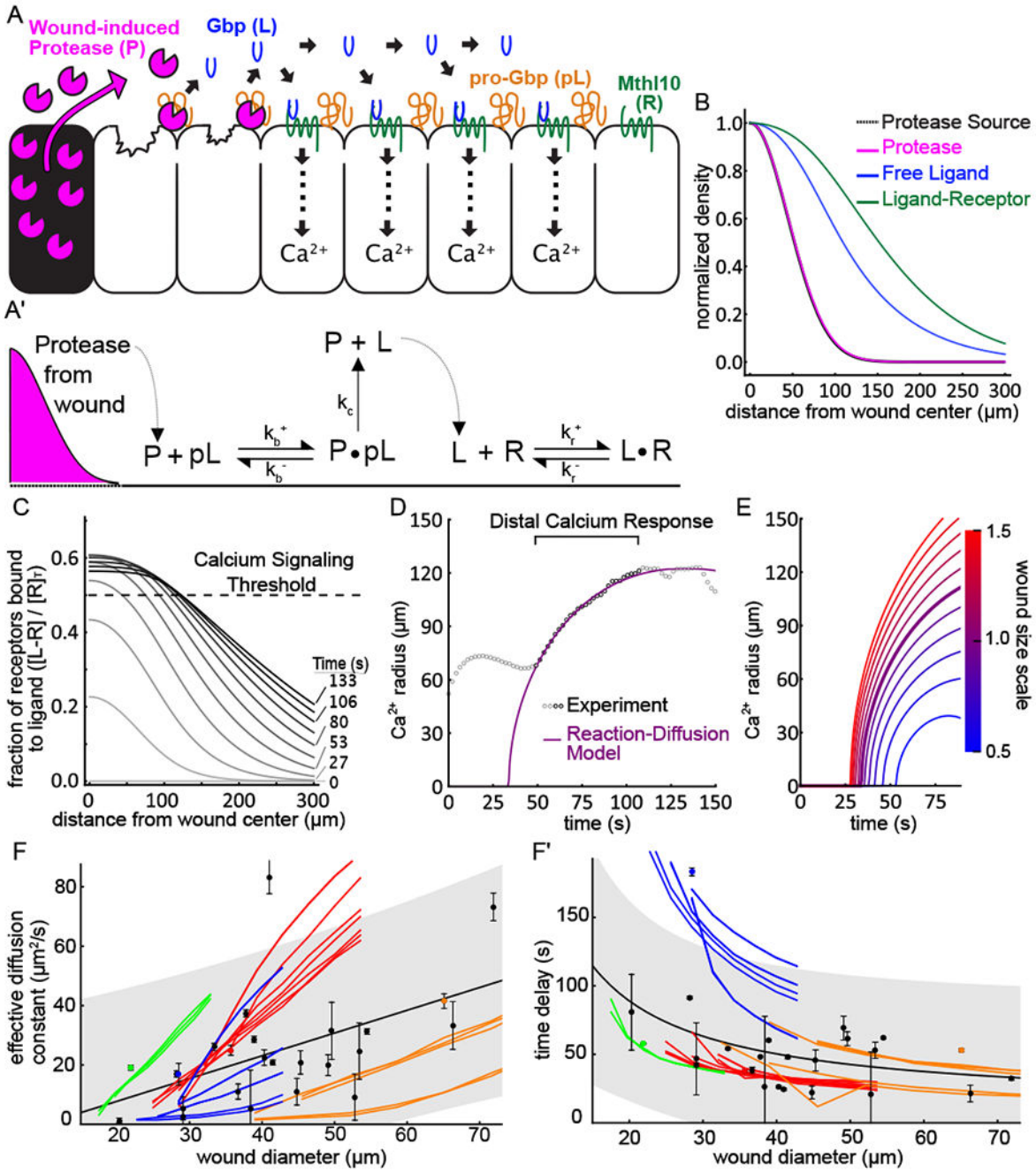

Figure 6: Reaction-diffusion (RD) model for epithelial wound detection.

(**A, A'**) Model schematic and reactions. Diffusible proteases (P) released from lysed and damaged cells cleave immobile pro-ligand (pL), releasing diffusible, activated ligand (L) that binds to its cognate cell-surface receptor (R). **(B)** RD model output of concentration of protease (pink line), free ligand (blue line), and ligand-receptor complex (green line) as a function of distance from the wound center 1 minute after wounding. Each line is normalized by the component's maximum concentration over all space 1 minute after wounding. The spatial extent of the protease source (black dashed line) is normalized so that

its maximum is 1. (**C**) Representative model output for the fraction of receptors bound to ligand as a function of distance from the wound at various times. Threshold for triggering calcium response is taken as 0.5 (dashed line). (**D**) Calcium signal radius versus time after wounding: experimental data (open circles), and RD model fit (purple line). (**E**) Calcium signal radius from the RD model for different simulated wound sizes; each line represents the impact of scaling the wound size for an otherwise fixed set of RD parameters determined from the best fit to an individual wound response. The bold line corresponds to a scale of 1.0 and matches the best fit line in panel D. **(F-F')** Experimental and modeled wound size dependence of the effective diffusion (F) and start time (F') of the distal calcium response. Experimental data (black dots) are taken from n = 26 wounds larger than 15 pm in diameter. Black line and shaded region indicate the best fit curve and single prediction 95% confidence interval respectively for a linear fit (F) and hyperbolic fit (F') to the data. Model results (colored lines) are determined by scaling the wound size from a best fit parameter set and then parameterizing the model outputs according to a delayed-diffusion model. Each color represents a fit to the same dataset (as in Fig. S3, S4), and each line corresponds to a different best fit parameter set. See also: Figures S3–5, Movie 9.

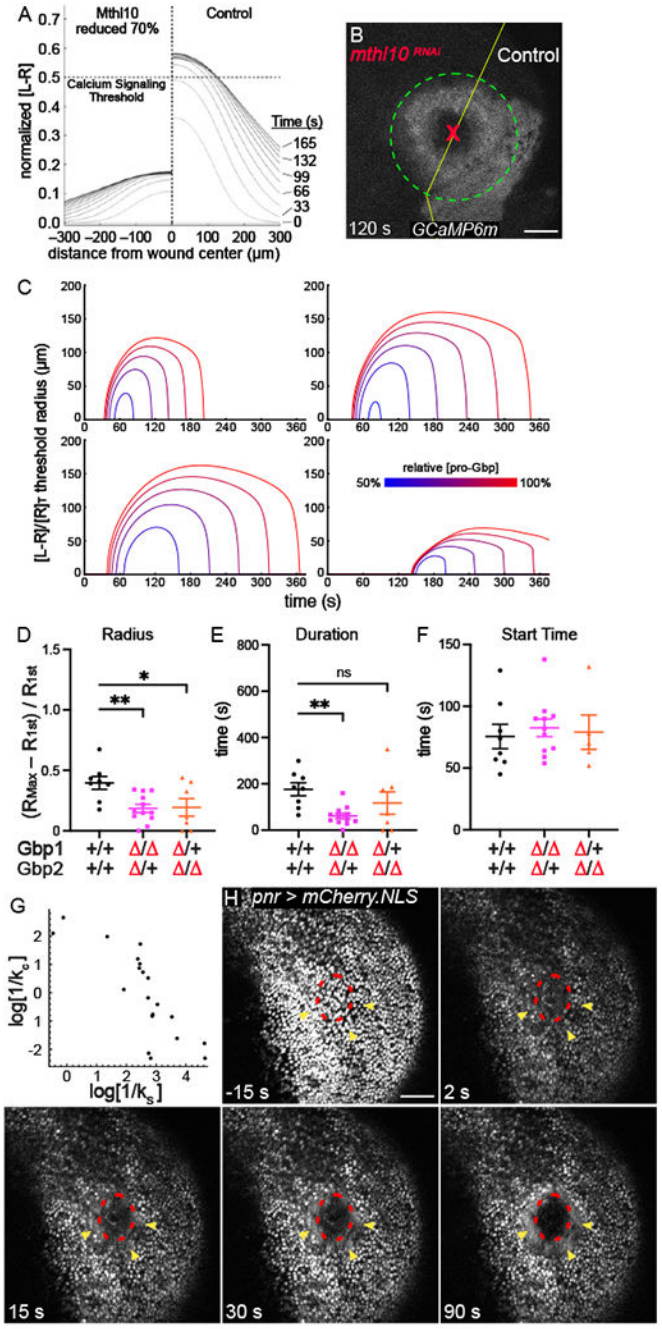

Figure 7: Reaction-diffusion (RD) model predictions and experimental validations.

(**A**) Representative RD model output for the normalized fraction of receptors bound to ligand as a function of distance from the wound at various times, with Mthl10 reduced on one side of the wound. The threshold for triggering calcium response is taken as 0.5 (dashed line). Negative distances (left side) correspond to the side with a reduced receptor level, and positive distances (right side) show the response on the control side with an unaltered receptor level. The signal does not reach the threshold on the side where Mlth10 is reduced, matching *in vivo* experimental data where *mthl10* is knocked down on one side (**B**). Scale

bar = 50 μm. (**C**) Model output for four parameter sets with varying initial concentration of extracellular pro-Gbp, showing sufficiently decreased levels of pro-Gbp are predicted to decrease the radius and duration of the calcium response, a result not observed in Fig. 3. (**D–F**) Post-hoc experiments performed on trans-heterozygous pupae expressing one allele of either *Gbp1* or *Gbp2* while null for the other. The distal calcium response radius is significantly decreased in both conditions (**D**), while the signal duration is decreased in the condition lacking both copies of *Gbp1* (**E**). Interestingly, the start times (**F**) were unchanged, as predicted in **C**. Statistical analysis by one-way ANOVA, multiple comparisons WRT control group, *$p<0.05$, **$p<0.01$. (G) Time constant of pro-ligand cleavage ($1/k_c$) is inversely correlated with the time constant of protease release and activation ($1/k_S$). The model predicts that a rapid pro-ligand cleavage will only occur if the protease is released and activated slowly over time, or in rare cases a rapid protease release can occur but only if the pro-ligand cleavage occurs slowly. In both cases, the triggering signal must build up slowly, indicating that cells lyse and protease accumulates progressively over time after wounding, rather than all at once. **(H)** The black region devoid of mCherry.NLS signal corresponds to the region of fully lysed cells. Cells lyse progressively over time during the first 90 s following wounding, expanding to a region indicated by the red dotted circle. Yellow arrowheads indicate cells with damaged nuclear membranes, which release nuclear-localized mCherry from nuclei into the cytosol, a process which also appears to occur progressively. Scale bar = 50 μm.

KEY RESOURCES TABLE

REAGENT or RESOURCE	SOURCE	IDENTIFIER
Antibodies		
Bacterial and virus strains		
Biological samples		
Chemicals, peptides, and recombinant proteins		
Schneider's Drosophila Media	Thermo Fisher	Cat#21720024
Clostripain	Alfa Aesar, Thermo Fisher	Cat#J61362
Trypsin	Gibco, Life Technologies	Cat# 25300054
Gbp1–5	This paper	https://www.genscript.com/peptide-services.html?
Bbsl	New England Biolabs	Cat#R3539S
Critical commercial assays		
Deposited data		
Experimental models: cell lines		
Experimental models: organisms/strains		
See Table S1	Various	N.A.
See Table S2	Various	N.A.
Oligonucleotides		
$Gbp1^{\Delta}$ gRNA#1: ATTTGCTCCCATCATTTATC	Millipore Sigma	https://www.sigmaaldrich.com/
$Gbp1^{\Delta}$ gRNA#2: CGGAAAACGATGCAGAAAGC	Millipore Sigma	https://www.sigmaaldrich.com/
$Gbp2^{3\Delta FS}$ gRNA#1: GAATATTCAACGCTGCCGTT	Millipore Sigma	https://www.sigmaaldrich.com/
$Gbp2^{3\Delta FS}$ gRNA#2: AATTCCATACAACCGCGTCC	Millipore Sigma	https://www.sigmaaldrich.com/
Recombinant DNA		
pGP-CMV-GCaMP6m	Chen, et al., 2013	Addgene Plasmid #40754
Actin5c Promoter	Struhl and Basler, 1993	N.A.
pBPw.Act5CP-GCaMP6m	This paper	N.A.
pCFD5 vector	Addgene	Plasmid #73914
Software and algorithms		
FIJI	Schindelin, et al., 2012	https://imagej.net/Fiji
Microsoft Excel	Microsoft	https://www.microsoft.com/en-us/microsoft-365/excel
GraphPad Prism 9	Graphpad	https://www.graphpad.com/scientific-software/prism/
Affinity Designer	Affinity Serif	https://affinity.serif.com/en-us/designer/
Inkscape	Inkscape	https://inkscape.org/
MATLAB	MathWorks	https://www.mathworks.com/products/matlab.html
Wolfram Mathematica	Wolfram	https://www.wolfram.com/mathematica/

REAGENT or RESOURCE	**SOURCE**	**IDENTIFIER**
CRISPR Fly Design	Port, et al., 2014	www.crisprflydesign.org
JBrowse	Skinner, et al. 2009	https://flybase.org/jbrowse/
Other		
Cell Signaling Technologies Protease inhibitor cocktail	Cell Signaling Technology	Cat#5871S
MS-Safe Protease and Phosphatase inhibitor	Millipore Sigma	MSSAFE
Protease Inhibitor Cocktail Set III	Millipore Sigma	Cat#539134
Protease Inhibitor Cocktail Set VI	Millipore Sigma	539133